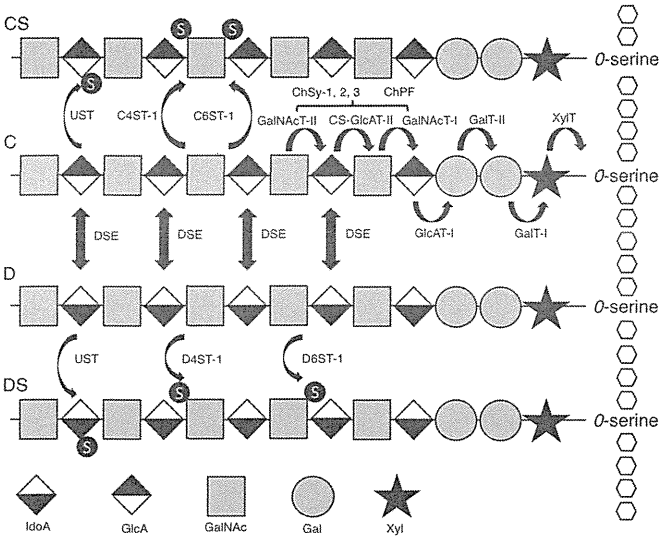

Fig. 4 Biosynthesis of dermatan sulfate (DS) and chondroitin sulfate (CS) is initiated by the synthesis of a tetrasaccharide linker egion, glucuronic acid β1-3galactoseβ1-3galactoseβ1-4xyloseβ1-*O*-(GlcA-Gal-Gal-Xyl-), onto serine residues of specific core proteins of proteoglycans by β-xylosyltransferase (XylT), β1,4-galactosyl transferase-I (GalT-I), β1,3-galactosyltransferase-II (GalT-II), and β1,3-glucuronosyltransferase-I (GlcAT-I), respectively. Subsequently, a repeating disaccharide region [*N*-acetyl-D-galactosamine(GalNAc)-GlcA]$_n$ of chondroitin is elongated by the actions of *N*-acetyl-D-galactosaminyltransferase-I (GalNAcT-I), *N*-acetyl-D-galactosaminyltransferase-II (GalNAcT-II), and CS-glucuronyltransferase-II (CS-GlcAT-II) encoded by chondroitin synthase-1, -2, and -3 and chondroitin polymerizing factor. CS chains are matured by modifications by chondroitin 4-*O*-sulfotransferase (C4ST), chondroitin 6-*O*-sulfotransferase (C6ST), and uronyl 2-*O*- sulfotransferase (UST). A disaccharide-repeating region of dermatan is synthesized through epimerization of a carboxyl group at C5 from GlcA to L-iduronic acid (IdoA) by DS epimease (DSE). A mature DS chain is synthesized through sulfation by dermatan 4-*O*-sulfotransferase (D4ST), dermatan 6-*O*-sulfotransferase (D6ST), and UST. (Reproduced from Kosho et al. Handbook of Glycosyltransferases and related genes, 2nd edition. 2014; 1135–48, with permission from Springer Japan.)

Table 2) and to 14.5% in a patient with the homozygous mutation P281L (patient 14), compared with each age- and sex-matched control (Fig. 5a).[7] Disaccharide composition analysis of CS/DS chains isolated from the affected skin fibroblasts in these two patients showed a negligible amount of DS and excess amount of CS (Fig. 5b),[7] which was suggested to result from impaired 4-*O*-sulfation lock due to CHST14/D4ST1 deficiency followed by back-epimerization from IdoA to GlcA.[5,7,20] A major DS-PG in the skin, decorin, was also investigated. Decorin consists of a core protein and a single GAG chain that plays an important role in assembly of collagen fibrils, possibly through an electrostatic interaction between decorin DS chains and adjacent collagen fibrils.[25] GAG chains of decorin from the affected skin fibroblasts contained exclusively CS and no DS disaccharides, while those from the controls contained mainly DS disaccharides (approx. 95%; Fig. 5c).[7] This was also demonstrated by Syx *et al.*[20]

Pathological abnormalities

Pathological findings are reportedly variable. Light microscopy of a skin specimen using hematoxylin and eosin (HE), elastica, and periodic acid–Schiff staining by Dündar *et al.* showed a normal appearance.[5] HE-stained skin specimens of our patients, however, showed that fine collagen fibers were present predominantly in the reticular to papillary dermis with marked reduction of normally thick collagen bundles (Fig. 6a,b).[7]

Transmission electron microscopy (TEM) of a skin specimen by Dündar *et al.* showed that collagen fibrils were normally packed and round with a normal diameter and contour.[5] TEM of skin specimens of our patients, however, showed that collagen fibrils in affected skin specimens were dispersed in the reticular dermis, in contrast to the regularly and tightly assembled collagen fibrils observed in the controls.[7] Each collagen fibril in the affected skin specimens was smooth and round, did not vary in size and shape, and was similar to each collagen fibril of the controls (Fig. 6c,d).[7] TEM of a skin specimen by Malfait *et al.* showed small-sized collagen bundles comprising collagen fibrils with variable diameters separated by irregular interfibrillar spaces; flower-like collagen fibrils; granulofilamentous material throughout the dermis, within the collagen bundles, and in the interstitial area; and elongated and/or dilated endoplasmic reticula in fibroblasts.[8]

Immunofluorescent staining of several extracellular matrix components in dermal fibroblast cultures of patients was

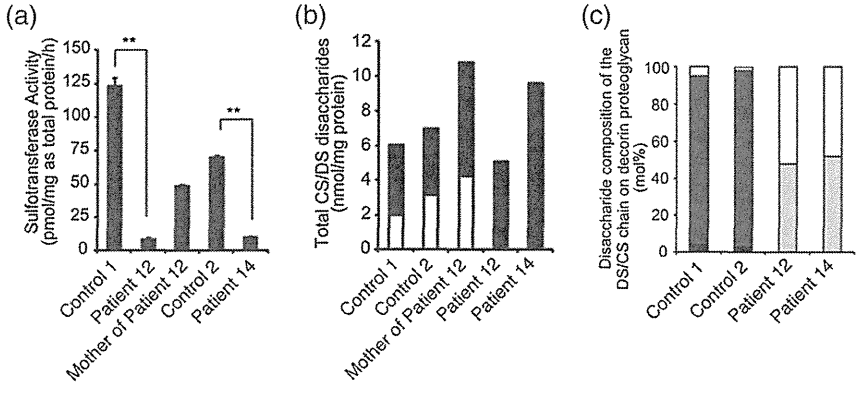

Fig. 5 Glycobiology. Control 1 is patient 12's age- and sex-matched control. Control 2 is patient 14's age- and sex-matched control. Patient number is according to Table 2. (a) Sulfotransferase activities of skin fibroblasts. (b) Total amounts of chondroitin sulfate (CS) and dermatan sulfate (DS) derived from skin fibroblasts. Total disaccharide content in (black box) CS and (white box) DS. (c) Proportion of the disaccharide units in the CS/DS hybrid chains in decorin secreted by the fibroblasts. (white box) GlcUA-GalNAc (4S) and (light gray box) GlcUA-GalNAc (6S), both comprising CS; (dark gray box) IdoUA-GalNAc (4S) and (black box) IdoUA (2S)-GalNAc (4S), both comprising DS. (Reproduced from Miyake et al. Hum. Mutat. 2010; 31: 966–74, with permission from Wiley-Liss, Inc.)

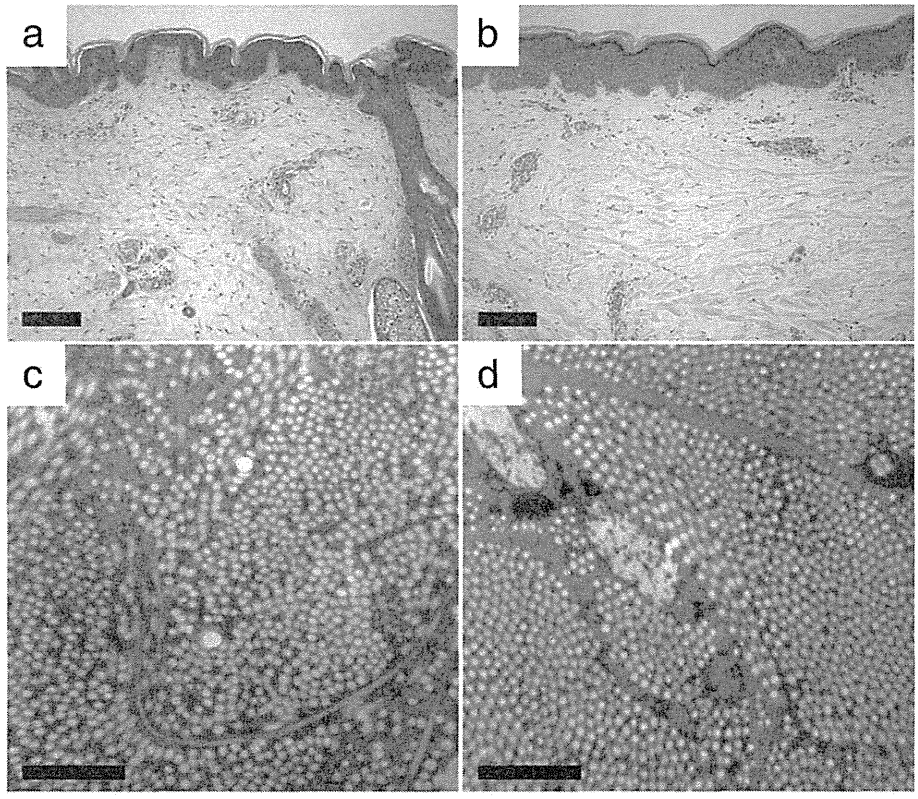

Fig. 6 Pathology. (a) Light microscopy of a hematoxylin- and eosin-stained skin specimen of patient 16 in Table 2 and (b) that of her age- and sex-matched control. Scale bars, 500 μm. (c) Electron microscopy of a skin specimen of patient 16 and (d) that of the control. Scale bars,1 μm. (Reproduced from Miyake et al. Hum. Mutat. 2010; 31: 966–74, with permission from Wiley-Liss, Inc.)

performed to evaluate the effect of D4ST1 deficiency on the general assembly and organization of the extracellular matrix. Mendoza-Londono *et al.* showed that staining for CS was higher in a patient's fibroblasts than normal fibroblasts, and that staining for collagen types I and III as well as fibrillin-1 was lower in the patient's fibroblasts than normal fibroblasts.[17] Syx *et al.* showed that staining for fibronectin, a glycoprotein previously shown to interact with decorin,[26] was reduced in the patients' fibroblasts with a less organized structure than the linear pattern observed in normal fibroblasts; that staining for collagen types I and III was poorly organized and more diffuse, with disruption of the linear arrangement in the patients' fibroblasts compared with normal fibroblasts; and that staining for collagen V, which forms heterotypic fibrils with collagen type I, was more fragmented in patients' fibroblasts than the interconnected pattern in normal fibroblasts.[20]

Underlying pathophysiology

In view of these glycobiological and pathological findings, skin fragility in patients with CHST14/D4ST1 deficiency was suggested to be caused by impaired assembly of collagen fibrils caused by the replacement of a DS with a CS chain of decorin. Complete replacement of a DS chain with a CS chain, caused by deficiency of CHST14/D4ST1, might result in alterations in the electrostatic binding of decorin to collagen fibrils,[25] followed by difference in the spatial relationship between collagen fibrils and decorin (Fig. 7a,b).[4,22,23]

Carbohydrate sulfotransferase 14/D4ST1 deficiency is the first human disorder found to specifically affect the biosynthesis of DS.[27] Clinical features of this disorder, namely congenital malformations and progressive multisystem fragility-related complications, suggest that CHST14/D4ST1 and, more funda-

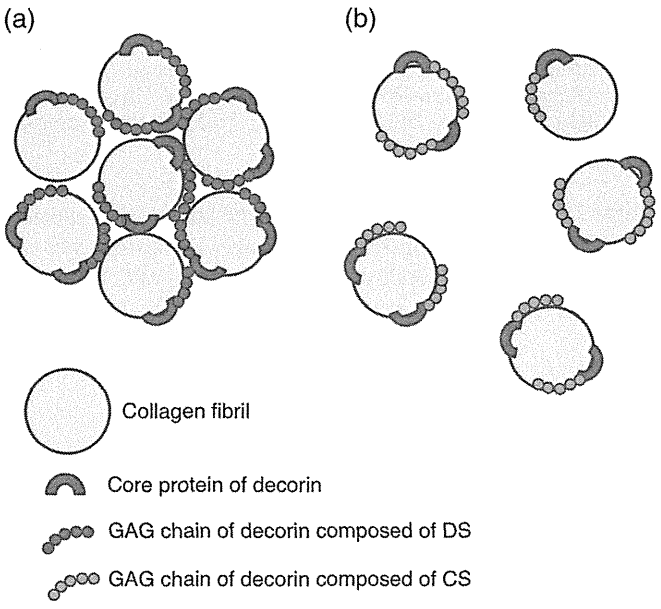

Fig. 7 Putative pathophysiology of CHST14/D4ST1 deficiency. Schematic diagram of binding model of decorin to collagen fibrils.[25] Putative spatial relationship between collagen fibrils and decorin in skin specimens of (a) normal control subjects and (b) patients with EDS caused by CHST14/D4ST1 deficiency (Reproduced from Kosho. Shinshu Med. J. 2011; 59: 305–19, with permission from Shinshu Medical Society.)

mentally, DS, plays a crucial role in fetal development and maintenance of connective tissues in multiple organs. Glycobiological and pathological evidence obtained from patients with CHST14/D4ST1 deficiency indicates that CHST14/D4ST1 has a substantial role in regulating the CS/DS disaccharide composition of a GAG chain of decorin (and probably other DS-PG). This would in turn exert various biological effects such as appropriate assembly of collagen fibrils mediated by decorin. Ubiquitous expression of *CHST14* also suggests multisystem effects of the enzyme.[23]

Knockout Chst14/D4st1-deficient (*Chst14*$^{-/-}$) mice were generated by homologous recombination and targeting of the only coding exon (exon 1) of *Chst14*.[28,29] Phenotypic analysis of the F2 mice suggested that the mutation affected growth (reduced weight/length) and bone metabolism (reduced bone volume/thickness/density of lumbar vertebrae).[28] *Chst14*$^{-/-}$ mice had decreased neurogenesis and diminished proliferation of neural stem cells accompanied by increased expression of glutamate aspartate transporter and epidermal growth factor compared with both wild-type (*Chst14*$^{+/+}$) controls and Chst11/C4st1-deficient (*Chst11*$^{-/-}$) mice.[29] Additionally, *Chst14*$^{-/-}$ mice had a smaller body mass, reduced fertility, a kinked tail, and increased skin fragility compared with their wild-type (*Chst14*$^{+/+}$) littermates; brain weight and gross anatomy were unaffected. Schwann cells from *Chst14*$^{-/-}$ mice formed longer processes *in vitro* and proliferated more than those from *Chst14*$^{+/+}$ mice. After femoral nerve transection/suture, functional recovery and axonal regrowth in *Chst14*$^{-/-}$ mice were initially accelerated, but the final outcome 3 months after injury was not better than that in *Chst14*$^{+/+}$ littermates. DS-PG, produced by Chst14/D4st1, were therefore suggested to contribute to the regeneration-restricting environment in the adult mammalian nervous system.[30]

Human D4ST1 deficiency

Discussions about the delineation of human CHST14/D4ST1 deficiency followed independent identification of this disorder as "adducted thumb–clubfoot syndrome",[5] "EDS, Kosho type",[6,7] and "musculocontractural EDS".[8] Janecke *et al.* proposed that these three conditions constitute a clinically recognizable and genetically identical type of connective tissue disorder and that the disorder should not be categorized as a form of EDS, but be collectively termed "dermatan sulfate-deficient adducted thumb–clubfoot syndrome" to avoid possible confusion for both clinicians and researchers.[31] Clinically, the proposal was based on the presence of atypical findings in patients with EDS (multiple congenital malformations such as facial dysmorphism, cleft lip/palate, intestinal abnormalities, and renal abnormalities, as well as other features such as nephrolithiasis and muscle hypotonia) in addition to typical features such as joint laxity, skin hyperextensibility/fragility, and bleeding diathesis; etiologically, the proposal was based on molecular differences.[31]

Five days before the aforedescribed publication by Janecke *et al.*,[31] we had submitted an article describing the detailed clinical findings and courses of two additional unrelated patients and presenting a comprehensive review of all reported patients at that time.[16] In the article, we also concluded that "adducted thumb–clubfoot syndrome", "EDS, Kosho type", and "musculo contractural EDS" represent a single clinically recognizable disorder characterized by multiple congenital malformations and progressive multisystem fragility-related complications; we thus proposed the term "D4ST1-deficient EDS".[16]

Furthermore, we published a reply to Janecke *et al.*[31] explaining the reasons why we categorized CHST14/D4ST1 deficiency as a form of EDS.[32] Clinically, the disorder satisfies all the hallmarks of EDS (skin hyperextensibility, joint hypermobility, and tissue fragility),[1] and prevention and treatment of multisystem fragility-related complications is the primary management goal.[32] "Adducted thumb–clubfoot syndrome" is a helpful term to detect and diagnose patients at birth, but whether it is appropriate for life-long management remains questionable.[32] Clinical manifestations extending beyond the core features of EDS are not excluded from the definition of EDS; wide clinical variability is seen in EDS, such as muscle hypotonia and chronic pain in most of the types, talipes equinovarus and facial characteristics in the vascular type, and congenital hip dislocation in the arthrochalasia type.[3,33] Etiologically, multisystem fragility was suggested to be caused by impaired assembly of collagen fibrils resulting from loss of DS in the decorin GAG side chain, which could justify terming the disorder a form of EDS.[32] Therefore, we again proposed that the term "D4ST1-deficient EDS (DDEDS; adducted thumb–clubfoot syndrome)" would be preferable, presenting a summary of clinical manifestations of the disorder (Table 3).[32]

Currently, the disorder is registered in OMIM (http://omim.org/) as "EDS, musculocontractural type 1 (EDSMC1)" (601776) to distinguish a subsequently identified form of EDS caused by recessive loss-of-function mutations in the DS epimerase-1 (DSE) gene (*DSE*) that is registered as "EDS, musculocontractural type 2 (EDSMC2)" (615539).[20,34] DSE is a critical enzyme to synthesize a disaccharide-repeating region of dermatan from that of chondroitin through epimerization of a carboxyl group at C5 from GlcA to IdoA (Fig. 4).[23] To date, only three patients from two families have been reported, who share several clinical features with CHST14/D4ST1-deficient patients, including craniofacial characteristics, clubfeet, long and slender fingers with contractures, muscle weakness; smooth, hyperextensible, and translucent skin; and large subcutaneous hematomas.[20] They were reported to lack severe urological, gastrointestinal, respiratory, and ocular complications frequently observed in patients with CHST14/D4ST1-deficiency.[20,34] Disaccharide composition analysis of CS/DS chains from cultured skin fibroblasts in those with DSE deficiency detected a minor fraction of DS, in contrast with absent DS in those with CHST14/D4ST1-deficiency; which could be attributable to residual activity of mutant DSE or to partially compensating dermatan sulfate epimerase-like (DSEL/DSE2), a protein with DSE activities encoded by *DSEL/DSE2* with significant homology with *DSE*.[20,34] It is at present an unsolved problem as to whether DSE deficiency would be clinically delineated from CHST14/D4ST1 deficiency.[20]

OMIM also presents alternative titles to EDSMC1, including "adducted thumb, clubfoot, and progressive joint and skin laxity syndrome", "EDSVIB", "adducted thumb–clubfoot syndrome", "Dündar syndrome", and "arthrogryposis, distal, with peculiar facies and hydronephrosis".

Table 3 Clinical manifestations of EDS caused by CHST14/D4ST1 deficiency

Craniofacial	Cardiovascular
Large fontanelle (early childhood)	Congenital heart defects (ASD)
Hypertelorism	Valve abnormalities (MVP, MR, AR, ARD)
Short and downslanting palpebral fissures	Large subcutaneous hematomas
Blue sclerae	Gastrointestinal
Short nose with hypoplastic columella	Constipation
Ear deformities (prominent, posteriorly rotated, low-set)	Diverticula perforation
Palatal abnormalities (high, cleft)	Respiratory
Long philtrum and thin upper lip	Pneumothorax/pneumohemothorax
Small mouth/micro-retrognathia (infancy)	Urogenital
Slender face with protruding jaw (from school age)	Nephrolithiasis/cystolithiasis
Asymmetric face (from school age)	Hydronephrosis
Skeletal	Dilated/atonic bladder
Marfanoid habitus/slender build	Inguinal hernia
Congenital multiple contractures (fingers, wrists, hips, feet)	Cryptorchidism
Recurrent/chronic joint dislocations	Poor breast development
Pectus deformities (flat, excavated)	Ocular
Spinal deformities (scoliosis, kyphoscoliosis)	Strabismus
Peculiar fingers (tapering, slender, cylindrical)	Refractive errors (myopia, astigmatism)
Progressive talipes deformities (valgus, planus, cavum)	Glaucoma/elevated intraocular pressure
Cutaneous	Microcornea/microphthalmia
Hyperextensibility/redundancy	Retinal detachment
Bruisability	Hearing
Fragility/atrophic scars	Hearing impairment
Fine/acrogeria-like palmar creases	Neurological
Hyperalgesia to pressure	Ventricular enlargement/asymmetry
Recurrent subcutaneous infections/fistula	Development
	Hypotonia/gross motor delay.

AR, aortic valve regurgitation; ARD, aortic root dilation; ASD, atrial septal defect; D4ST1, dermatan 4-*O*-sulfotransferase-1; MR, mitral valve regurgitation; MVP, mitral valve prolapse. (Reproduced from Kosho et al. Hum. Mutat. 2011; 32: 1507–9, with permission from Wiley Periodicals Inc.)

Health-care guidelines

Diagnosis

Carbohydrate sulfotransferase 14/D4ST1 deficiency is typically noticed at birth or in early childhood based on characteristic craniofacial and skeletal features. The author proposes use of the following major clinical criteria: (i) "characteristic craniofacial features" including a large fontanelle, hypertelorism, short and downslanting palpebral fissures, blue sclerae, short nose with hypoplastic columella, low-set and rotated ears, high palate, long philtrum, thin upper lip vermilion, small mouth, and micro-retrognathia, all of which are evident from birth to early childhood; (ii) "multiple congenital contractures" including adduction–flexion contractures and/or talipes equinovarus (clubfoot); and (iii) "characteristic cutaneous features" including hyperextensibility, bruisability, fragility with atrophic scars, and palm wrinkles. Molecular genetic testing for *CHST14* is recommended in patients with at least two major clinical criteria (characteristic craniofacial features and multiple congenital contractures at birth or in early childhood; or multiple congenital contractures and characteristic cutaneous features from adolescence to adulthood). Minor clinical criteria that support the clinical diagnosis include skeletal abnormalities (recurrent/chronic dislocations, pectus deformities [flat, excavated], spinal deformities [scoliosis, kyphoscoliosis], peculiar fingers [tapering, slender, cylindrical], progressive talipes deformities [valgus, planus, cavum]), vascular abnormalities (large subcutaneous hematomas), visceral abnormalities (constipation, diverticula, pneumothorax/pneumohemothorax, nephrolithiasis/cystolithiasis, hydronephrosis, cryptorchidism in boys), and ophthalmological abnormalities (strabismus, refractive errors [myopia, astigmatism], glaucoma/elevated intraocular pressure).

Differential diagnoses of CHST14/D4ST1 deficiency include conditions that could present early onset fragility-related manifestations as well as congenital contractures: DSE deficiency that might be a milder form of the disorder;[20,34] the progeroid type EDS (130070, 615349) caused by recessive mutations in the xylosylprotein 4-β-galactosyltransferase, polypeptide 7 (*B4GALT7*)[35] or the UDP-Gal, β-Gal β-1,3-galactosyltransferase, polypeptide 6 (*B3GALT6*),[36,37] respectively, both encoding galactosyltransferases that form a tetrasaccharide linker region indispensable to the initiation of CS/DS biosynthesis; kyphoscoliosis-type EDS (MIM 225400) caused by recessive mutations in the lysyl hydroxylase gene (*PLOD*);[38] spondylocheirodysplastic EDS (612350) caused by recessive mutations in a membrane-bound zinc transporter encoded by *SLC39A13*;[39] EDS with progressive kyphoscoliosis, myopathy, and hearing loss (614557) caused by recessive mutations in the FK506-binding protein 14 (*FKBP14*);[40] Loeys–Dietz syndrome (609192, 610168) caused by heterozygous mutations in the transforming growth factor-β receptor, type I gene (*TGFBR1*) and type II (*TGFBR2*), respectively;[41] severe and rapidly progressive form of Marfan syndrome, sometimes termed "neonatal Marfan syndrome" caused by heterozygous mutations in the center portion of the fibrillin 1 gene (*FBN1*).[42]

Management

Initial screening for congenital cardiac, ocular, and renal abnormalities and hearing loss is recommended. In infancy, orthopedic intervention (e.g. serial plaster casts or surgery) for talipes equinovarus and physical therapy for motor developmental delay are the primary management techniques. Laxatives and/or enemas are considered in patients with constipation. Surgical fixation is considered for cryptorchidism in boys. Regular checkups for ophthalmological (strabismus, refractive errors, glaucoma), otological (otitis media with effusion, hearing impairment), urological (urination, bladder enlargement), and cardiovascular (valve abnormalities, aortic root dilation) problems is recommended. After walking independently, attention must be given to progressive foot deformities and trauma that could cause skin lacerations, joint dislocations, or large subcutaneous hematomas. Intranasal DDAVP after trauma is considered to prevent large subcutaneous hematomas. From adolescence, assessment of spinal deformities (scoliosis, kyphoscoliosis) and secondary sex characteristics (breast development in girls and gonadal function in boys) is recommended. In adulthood, appropriate treatment may be needed for occasional emergency complications including pneumothorax or pneumohemothorax, large subcutaneous hematomas, and diverticular perforation. A wrist-type sphygmomanometer is preferable for patients with hyperalgesia to pressure.[16]

Ongoing projects and future perspectives

To revise the nosology based on the most current clinical and molecular information on the major types and additional forms of EDS, the international consortium for EDS (ICEDS) was established in 2013 in Paris, following the First International Symposium on EDS held from 8 to 11 September 2012 in Ghent, Belgium. The author was selected as a member of this consortium, is responsible for delineation of this form of EDS caused by CHST14/D4ST1 deficiency, and is working together with colleagues worldwide to complete the revision of the nosology in 2016.

Our clinical and basic research on CHST14/D4ST1 deficiency was promoted from 2009 to 2013 by the grant "Research on Intractable Diseases" from the Ministry of Health, Labour and Welfare, Japan. In 2015, our activities were selected for the "Practical Research Project for Rare/Intractable Diseases, Japan Agency for Medical Research and Development (AMED)". Considering that patients with CHST14/D4ST1 deficiency suffer from progressive multisystem fragility-related manifestations (decreased quality of life due to progressive spinal and foot deformities and potentially fatal large subcutaneous hematomas), establishment of a comprehensive and detailed natural history and of health-care guidelines, as well as further elucidation of the pathophysiology in view of future etiology-based therapy, are crucial. In this context, the author is leading an international collaborative study involving the collection of updated clinical information of previously reported patients and detailed information of unreported patients worldwide. The study also involves coordination of comprehensive basic research with Japanese colleagues using patient samples, induced-pluripotent stem cells from patient skin fibroblasts, and knockout mice.

Acknowledgments

The author is thankful to the patients and their families. The author is also grateful to Dr Shuji Mizumoto, Meijo University, for his critical comments on this review, and all colleagues in Shinshu University School of Medicine, the AMED, and the ICEDS. Grant sponsors are as follows: Practical Research Project for Rare/Intractable Diseases, Japan Agency for Medical Research and Development (AMED) (105); Grant-in-Aid for Scientific Research (C) from the Ministry of Education, Culture, Sports, Science and Technology of Japan (25460405); Research on Intractable Diseases, Ministry of Health, Labour and Welfare, Japan (073); Medical Research Encouragement Prize of the Japan Medical Association (2013); and Japan Foundation for Pediatric Research (2014).

Disclosure

The authors declare no conflicts of interest.

References

1 Steinmann B, Royce PM, Superti-Furga A. The Ehlers–Danlos syndrome. In: Royce PM, Steinmann B (eds). *Connective Tissue and its Heritable Disorders*. Wiley-Liss, New York, 2002; 431–523.
2 Mao JR, Bristow J. The Ehlers–Danlos syndrome: On beyond collagens. *J. Clin. Invest.* 2001; **107**: 1063–9.
3 Beighton P, De Paepe A, Steinmann B, Tsipouras P, Wenstrup R. Ehlers–Danlos syndromes: Revised nosology, Villefranche, 1997. *Am. J. Med. Genet.* 1998; **77**: 31–7.
4 Kosho T. Discovery and delineation of dermatan 4-*O*-sulfotransferase-1 (D4ST1)-deficient Ehlers-Danlos syndrome. In: Oiso N, Kawada A (eds). *Current Genetics in Dermatology*. InTech, Croatia, 2013; 73–86.
5 Dündar M, Müller T, Zhang Q *et al.* Loss of dermatan-4-sulfotransferase 1 function results in adducted thumb-clubfoot syndrome. *Am. J. Hum. Genet.* 2009; **85**: 873–82.
6 Kosho T, Miyake N, Hatamochi A *et al.* A new Ehlers–Danlos syndrome with craniofacial characteristics, multiple congenital contractures, progressive joint and skin laxity, and multisystem fragility-related manifestations. *Am. J. Med. Genet. Part A.* 2010; **152A**: 1333–46.
7 Miyake N, Kosho T, Mizumoto S *et al.* Loss-of-function mutations of *CHST14* in a new type of Ehlers–Danlos syndrome. *Hum. Mutat.* 2010; **31**: 966–74.
8 Malfait F, Syx D, Vlummens P *et al.* Musculocontractural Ehlers–Danlos syndrome (former EDS type VIB) and adducted thumb clubfoot syndrome (ATCS) represent a single clinical entity caused by mutations in the dermatan-4-sulfotransferase 1 encoding *CHST14* gene. *Hum. Mutat.* 2010; **31**: 1233–9.
9 Dündar M, Demiryilmaz F, Demiryilmaz I *et al.* An autosomal recessive adducted thumb-club foot syndrome observed in Turkish cousins. *Clin. Genet.* 1997; **51**: 61–4.
10 Dündar M, Kurtoglu S, Elmas B *et al.* A case with adducted thumb and club foot syndrome. *Clin. Dysmorphol.* 2001; **10**: 291–3.
11 Sonoda T, Kouno K. Two brothers with distal arthrogryposis, peculiar facial appearance, cleft palate, short stature, hydronephrosis, retentio testis, and normal intelligence: A new type of distal arthrogryposis? *Am. J. Med. Genet.* 2000; **91**: 280–5.
12 Janecke AR, Unsinn K, Kreczy A *et al.* Adducted thumb-club foot syndrome in sibs of a consanguineous Austrian family. *J. Med. Genet.* 2001; **38**: 265–9.

13 Kosho T, Takahashi J, Ohashi H, Nishimura G, Kato H, Fukushima Y. Ehlers–Danlos syndrome type VIB with characteristic facies, decreased curvatures of the spinal column, and joint contractures in two unrelated girls. *Am. J. Med. Genet. Part A.* 2005; **138A**: 282–7.
14 Steinmann B, Gitzelmann R, Vogel A, Grant ME, Harwood R, Sear CH. Ehlers-Danlos syndrome in two siblings with deficient lysyl hydroxylase activity in cultured skin fibroblasts but only mild hydroxylysine deficit in skin. *Helv. Paediatr. Acta* 1975; **30**: 255–74.
15 Yasui H, Adachi Y, Minami T, Ishida T, Kato Y, Imai K. Combination therapy of DDAVP and conjugated estrogens for a recurrent large subcutaneous hematoma in Ehlers–Danlos syndrome. *Am. J. Hematol.* 2003; **72**: 71–2.
16 Shimizu K, Okamoto N, Miyake N *et al.* Delineation of dermatan 4-O-sulfotransferase 1 deficient Ehlers-Danlos syndrome: Observation of two additional patients and comprehensive review of 20 reported patients. *Am. J. Med. Genet. Part A.* 2011; **155A**: 1949–58.
17 Mendoza-Londono R, Chitayat D, Kahr WH *et al.* Extracellular matrix and platelet function in patients with musculocontractural Ehlers-Danlos syndrome caused by mutations in the *CHST14* gene. *Am. J. Med. Genet. Part A.* 2012; **158A**: 1344–54.
18 Voermans NC, Kempers M, Lammens M *et al.* Myopathy in a 20-year-old female patient with D4ST-1 deficient Ehlers-Danlos syndrome due to a homozygous CHST14 mutation. *Am. J. Med. Genet. Part A.* 2012; **158A**: 850–5.
19 Winters KA, Jiang Z, Xu W *et al.* Re-assigned diagnosis of D4ST1-deficient Ehlers-Danlos syndrome (adducted thumb-clubfoot syndrome) after initial diagnosis of Marden-Walker syndrome. *Am. J. Med. Genet. Part A.* 2012; **158A**: 2935–40.
20 Syx D, Van Damme T, Symoens S *et al.* Genetic heterogeneity and clinical variability in musculocontractural Ehlers-Danlos syndrome caused by impaired dermatan sulfate biosynthesis. *Hum. Mutat.* 2015; **36**: 535–47.
21 Evers MR, Xia G, Kang HG, Schachner M, Baeziger JU. Molecular cloning and characterization of a dermatan-specific *N*-acetylgalactosamine 4-O-sulfotransferase. *J. Biol. Chem.* 2001; **276**: s44–53.
22 Kosho T. Discovery and delineation of a new type of Ehlers-Danlos syndrome caused by dermatan 4-*O*-sulfotransferase deficiency. *Shinshu Med. J.* 2011; **59**: 305–19 (in Japanese).
23 Kosho T, Mizumoto S, Sugahara K. Carbohydrate (N-acetylgalactosamine 4-O) sulfotransferase 14 (CHST14). In: Taniguchi N, Honke K, Fukuda M, Narimatsu H, Yamaguchi Y, Angata T (eds). *Handbook of Glycosyltransferases and Related Genes*, 2nd edn. Springer, Berlin, 2014; 1135–48.
24 Mikami T, Mizumoto S, Kago N, Kitagawa H, Sugahara K. Specificities of three distinct human chondroitin/dermatan *N*-acetylgalactosamine 4-O-sulfotransferases demonstrated using partially desulfated dermatan sulfate as an acceptor: Implication of differential roles in dermatan sulfate biosynthesis. *J. Biol. Chem.* 2003; **278**: 36115–27.
25 Nomura Y. Structural changes in decorin with skin aging. *Connect. Tissue Res.* 2006; **47**: 249–55.
26 Schmidt G, Hausser H, Kresse H. Interaction of the small proteoglycan decorin with fibronectin. Involvement of the sequence NKISK of the core protein. *Biochem. J.* 1991; **280**: 411–4.
27 Zhang L, Müller T, Baenziger JU, Janecke AR. Congenital disorders of glycosylation with emphasis on loss of dermatan-4-sulfotransferase. *Prog. Mol. Biol. Transl. Sci.* 2010; **93**: 289–307.
28 Tang T, Li L, Tang J *et al.* A mouse knockout library for secreted and transmembrane proteins. *Nat. Biotechnol.* 2010; **28**: 749–55.
29 Bian S, Akyüz N, Bernreuther C *et al.* Dermatan sulfotransferase Chst14/D4st1, but not chondroitin sulfotransferase Chst11/C4st1, regulates proliferation and neurogenesis of neural progenitor cells. *J. Cell Sci.* 2011; **124**: 4051–63.
30 Akyüz N, Rost S, Mehanna A *et al.* Dermatan 4-O-sulfotransferase1 ablation accelerates peripheral nerve regeneration. *Exp. Neurol.* 2013; **247**: 517–30.
31 Janecke AR, Baenziger JU, Müller T, Dündar M. Loss of dermatan-4-sulfotransferase 1 (D4ST1/CHST14) function represents the first dermatan sulfate biosynthesis defect, "dermatan sulfate-deficient adducted thumb-clubfoot syndrome". *Hum. Mutat.* 2011; **32**: 484–5.
32 Kosho T, Miyake N, Mizumoto S *et al.* A response to: Loss of dermatan-4-sulfotransferase 1 (D4ST1/CHST14) function represents the first dermatan sulfate biosynthesis defect, "dermatan sulfate-deficient adducted thumb-clubfoot syndrome". Which name is appropriate, "adducted thumb-clubfoot syndrome" or "Ehlers-Danlos syndrome"? *Hum. Mutat.* 2011; **32**: 1507–9.
33 Voermans NC, van Alfen N, Pillen S *et al.* Neuromuscular involvement in various types of Ehlers–Danlos syndrome. *Ann. Neurol.* 2009; **65**: 687–97.
34 Müller T, Mizumoto S, Suresh I *et al.* Loss of dermatan sulfate epimerase (DSE) function results in musculocontractural Ehlers-Danlos syndrome. *Hum. Mol. Genet.* 2013; **22**: 3761–72.
35 Kresse H, Rosthoj S, Quentin E *et al.* Glycosaminoglycan-free small proteoglycan core protein is secreted by fibroblasts from a patient with a syndrome resembling progeroid. *Am. J. Hum. Genet.* 1987; **41**: 436–53.
36 Malfait F, Kariminejad A, Van Damme T *et al.* Defective initiation of glycosaminoglycan synthesis due to *B3GALT6* mutations causes a pleiotropic Ehlers-Danlos syndrome-like connective tissue disorder. *Am. J. Hum. Genet.* 2013; **92**: 935–45.
37 Nakajima M, Mizumoto S, Miyake N *et al.* Mutations in *B3GALT6*, which encodes a glycosaminoglycan linker region enzyme, cause a spectrum of skeletal and connective tissue disorders. *Am. J. Hum. Genet.* 2013; **92**: 927–34.
38 Yeowell HN, Steinmann B. Ehlers-Danlos syndrome, kyphoscoliotic form. In: Pagon RA, Adam MP, Ardinger HH *et al.* (eds). *GeneReviews® [Internet]*. University of Washington, Seattle, Seattle (WA), 1993–2015 2 Feb 2000 [updated 24 Jan 2013].
39 Giunta C, Elçioglu NH, Albrecht B *et al.* Spondylocheiro dysplastic form of the Ehlers-Danlos syndrome: An autosomal-recessive entity caused by mutations in the zinc transporter gene SLC39A13. *Am. J. Hum. Genet.* 2008; **82**: 1290–305.
40 Baumann M, Giunta C, Krabichler B *et al.* Mutations in *FKBP14* cause a variant of Ehlers-Danlos syndrome with progressive kyphoscoliosis, myopathy, and hearing loss. *Am. J. Hum. Genet.* 2012; **90**: 201–16.
41 Loeys BL, Dietz HC. Loeys-Dietz syndrome. In: Pagon RA, Adam MP, Ardinger HH *et al.* (eds). *GeneReviews® [Internet]*. University of Washington, Seattle, Seattle (WA), 1993–2015 28 Feb 2008 [updated 11 Jul 2013].
42 Dietz HC. Marfan syndrome. In: Pagon RA, Adam MP, Ardinger HH *et al.* (eds). *GeneReviews® [Internet]*. University of Washington, Seattle, Seattle (WA), 1993–2015 18 Apr 2001 [updated 12 Jun 2014].

JAPANESE DERMATOLOGICAL ASSOCIATION
THE JOURNAL OF DERMATOLOGY
doi: 10.1111/1346-8138.13273
Journal of Dermatology 2016; ●●: 1–2

LETTER TO THE EDITOR

Dermatan 4-*O*-sulfotransferase 1-deficient Ehlers–Danlos syndrome complicated by a large subcutaneous hematoma on the back

Dear Editor

A 13-year-old Japanese boy was admitted to our hospital for the treatment of a massive subcutaneous hematoma on the back. He was born to healthy parents, who were second cousins once removed. At birth, he was diagnosed with arthrogryposis. He had bilateral cryptorchidism, corrected surgically at the age of 1 year. Bilateral hydronephrosis was detected in infancy. At the age of 12 years, he developed perforation of colon diverticula. He had had multiple episodes of large subcutaneous hematomas.

The hematoma, which had enlarged rapidly after being hit by a chair, was painful and 23 cm × 28 cm in size (Fig. 1a,b). He had a round face with hypertelorism, short palpebral fissures, strabismus, a short nose with a hypoplastic columella, low-set and rotated ears, and microretrognathia (Fig. 1c). His skin was hyperextensible (Fig. 1d), redundant (Fig. 1a,b) and fragile (tearing after minor traumas) with atrophic scars on bilateral elbows (Fig. 1a), knees and buttocks. He had cylindrical and slender fingers with clinodactyly (Fig. 1e), and fine acrogeria-like palmar creases (Fig. 1f,g). He had hypermobility especially in small joints (Beighton score, 4), talipes valgus and planus (Fig. 1h,i), and rigidity of bilateral shoulders. Hematoxylin–eosin-stained light microscopy of the skin specimen from the upper arm showed that fine collagen fibers were predominant in the reticular to papillary dermis and normally thick collagen bundles were markedly reduced (Fig. 1j). Electron microscopy showed that the collagen fibrils were dispersed in the reticular dermis, whereas each collagen fibril was smooth and round, not varying in size and shape (Fig. 1l), as compared with a skin specimen from an age-matched control (Fig. 1k). He was suspected to have dermatan 4-*O*-sulfotransferase 1 (D4ST1)-deficient Ehlers–Danlos syndrome (DDEDS).[1] Direct sequencing of the gene, carbohydrate sulfotransferase 14 (*CHST14*) encoding D4ST1, detected a homozygous missense mutation (c.842C>T; p.Pro281Leu), commonly identified in Japanese patients (Fig. 1m).[2,3]

Dermatan 4-*O*-sulfotransferase 1-deficient EDS is a recently delineated form of EDS, clinically characterized by progressive multisystem fragility-related manifestations (skin hyperextensibility and fragility, progressive spinal and foot deformities, large subcutaneous hematoma) and various malformations (facial features, congenital eye/heart/gastrointestinal defects,

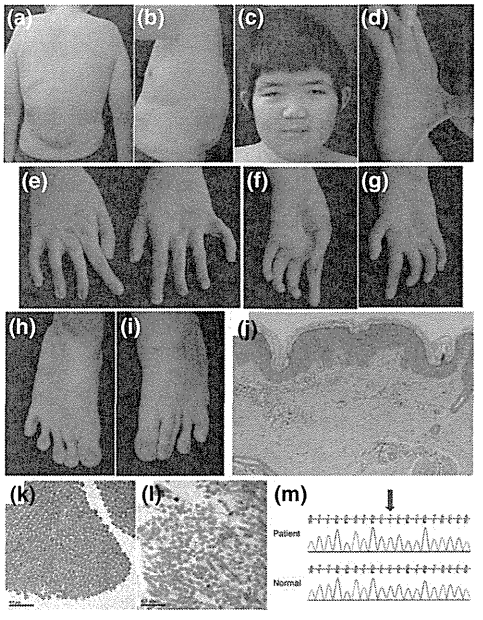

Figure 1. (a–i) Clinical photographs of the patient at admission. (a,b) A large subcutaneous hematoma on the back. (c) Facial appearance with hypertelorism, short palpebral fissures, strabismus, a short nose with a hypoplastic columella, low-set and rotated ears, and microretrognathia. (d) Skin hyperextensibility. (e) Cylindrical and slender fingers with clinodactyly. (f,g) Fine and acrogeria-like palmar creases. (h,i) Talipes valgus and planus. (j) Hematoxylin–eosin-stained light microscopy on the skin specimen from the upper arm of the patient, showing fine collagen fibers predominantly observed in the reticular to papillary dermis and normally thick collagen bundles markedly reduced. (k) Electron microscopy on the skin specimen from an age-matched control, showing tightly assembled collagen fibrils. (l) Electron microscopy on the skin specimen from the upper arm of the patient, showing collagen fibrils dispersed, in spite of each collagen fibril observed to be smooth and round, not varying in size and shape. (m) Sanger sequencing showing a homozygous C→T transition which results in proline to leucine substitution at amino acid position 281.

Correspondence: Masahiro Amano, M.D., Ph.D., Department of Dermatology, University of Miyazaki Faculty of Medicine, 5200 Kiyotakecho Kihara, Miyazaki City, Miyazaki 889-1692, Japan. Email: masahiro_amano@med.miyazaki-u.ac.jp
or
Tomoki Kosho, M.D., Department of Medical Genetics, Shinshu University School of Medicine, 3-1-1 Asahi, Matsumoto, Nagano 390-8621, Japan. Email: ktomoki@shinshu-u.ac.jp

congenital multiple contractures).[4] The progressive multisystem fragility is suggested to be caused by impaired assembly of collagen fibrils through loss of dermatan sulfate in the decorin, resulting from D4ST1 deficiency.[4] To date, 31 patients from 21 families have been reported.[1] The present patient, having typical facial, cutaneous and skeletal features, suffered from large subcutaneous hematomas. Recurrent large subcutaneous hematomas are one of the most serious complications in the disorder, though the pathophysiology is unknown. For the prevention, intranasal administration of 1-desamino-8-D-arginine vasopressin after traumas was described as effective in some patients.[5] DDEDS should be taken into consideration in case of pediatric patients diagnosed with arthrogryposis, accompanied by skin hyperextensibility and fragility, or patients with EDS who show characteristic facial and skeletal features and recurrent large subcutaneous hematomas.

ACKNOWLEDGMENTS: We are grateful to the patient and his family for their cooperation to this study. This study was supported by Practical Research Project for Rare/Intractable Diseases, Japan Agency for Medical Research and Development (#105) (K. T.) and Grant-in-Aid for Scientific Research (C) from the Ministry of Education, Culture, Sports, Science and Technology of Japan (#25460405) (K. T.).

CONFLICT OF INTEREST: None declared.

Kosuke MOCHIDA,[1] Masahiro AMANO,[1] Noriko MIYAKE,[2] Naomichi MATSUMOTO,[2] Atsushi HATAMOCHI,[3] Tomoki KOSHO[4]

[1]Department of Dermatology, University of Miyazaki Faculty of Medicine, Miyazaki, [2]Department of Human Genetics, Yokohama City University Graduated School of Medicine, Yokohama, [3]Department of Dermatology, School of Medicine, Dokkyo Medical University, Mibu, and [4]Department of Medical Genetics, Shinshu University School of Medicine, Matsumoto, Japan

REFERENCES

1 Kosho T. Discovery and delineation of dermatan 4-O-sulfotransferase-1 (D4ST1)-deficient Ehlers-Danlos syndrome. In: Oiso N, ed. *Current Genetics in Dermatology*. Croatia: InTech, 2013; 73–86.
2 Miyake N, Kosho T, Mizumoto S *et al.* Loss-of-function mutations of CHST14 in a new type of Ehles–Danlos syndrome. *Hum Mutat* 2010; **31**: 966–974.
3 Shimizu K, Okamoto N, Miyake N *et al.* Delineation of dermatan 4-O-sulfotransferase 1 deficient Ehlers-Danlos syndrome: observation of two additional patients and comprehensive review of 20 reported patients. *Am J Med Genet A* 2011; **155A**: 1949–1958.
4 Kosho T, Miyake N, Mizumoto S *et al.* A response to: loss of dermatan-4-sulfotransferase 1 (D4ST1/*CHST14*) function represents the first dermatan sulfate biosynthesis defect, "Dermatan sulfate-deficient adducted thumb-clubfoot syndrome". Which name is appropriate, "adducted thumb-clubfoot syndrome" or "Ehlers-Danlos syndrome"?. *Hum Mutat* 2011; **32**: 1507–1509.
5 Kosho T, Miyake N, Hatamochi A *et al.* A new Ehlers-Danlos syndrome with craniofacial characteristics, multiple congenital contractures, progressive joint and skin laxity, and multisystem fragility-related manifestations. *Am J Med Genet A* 2010; **152A**: 1333–1346.

SCIENTIFIC REPORTS

OPEN

TUBA1A mutation can cause a hydranencephaly-like severe form of cortical dysgenesis

Received: 13 March 2015
Accepted: 16 September 2015
Published: 23 October 2015

Setsuri Yokoi[1,3,*], Naoko Ishihara[2,3,*], Fuyuki Miya[4], Makiko Tsutsumi[1], Itaru Yanagihara[5], Naoko Fujita[1], Hiroyuki Yamamoto[3], Mitsuhiro Kato[6,†], Nobuhiko Okamoto[7], Tatsuhiko Tsunoda[4], Mami Yamasaki[8], Yonehiro Kanemura[9,10], Kenjiro Kosaki[11], Seiji Kojima[3], Shinji Saitoh[12], Hiroki Kurahashi[1] & Jun Natsume[3]

TUBA1A **mutations cause a wide spectrum of lissencephaly and brain malformations. Here, we report two patients with severe cortical dysgeneses, one with an extremely thin cerebral parenchyma apparently looking like hydranencephaly and the other with lissencephaly accompanied by marked hydrocephalus, both harbouring novel *de novo* missense mutations of *TUBA1A*. To elucidate how the various *TUBA1A* mutations affect the severity of the phenotype, we examined the capacity of the mutant protein to incorporate into the endogenous microtubule network in transfected COS7 cells by measuring line density using line extraction in an immunofluorescence study. The mutants responsible for severe phenotypes were found to incorporate extensively into the network. To determine how each mutant alters the microtubule stability, we examined cold-induced microtubule depolymerisation in fibroblasts. The depolymerisation of patients' fibroblasts occurred earlier than that of control fibroblasts, suggesting that microtubules bearing mutated tubulins are unstable. Both mutations are predicted to participate in lateral interactions of microtubules. Our data suggest that the *TUBA1A* mutations disrupting lateral interactions have pronounced dominant-negative effects on microtubule dynamics that are associated with the severe end of the lissencephaly spectrum.**

In the past two decades, it has become evident that the genes encoding cytoskeletal proteins are important in the developing brain[1]. Their importance was initially inferred from the identification of genes encoding microtubule-associated proteins (MAPs), such as *LIS1* (also known as *PAFAH1B1*) and *DCX*, which are mutated in the lissencephaly spectrum[2]. Several years later, new disorders associated with mutations in genes encoding for α- or β-tubulin were described[3–10]. The α- and β-tubulins are the major components of microtubules and are characterised by variable isotypes whose expressions are spatially

[1]Division of Molecular Genetics, Institute for Comprehensive Medical Science, Fujita Health University, Toyoake, Japan. [2]Department of Pediatrics, Fujita Health University School of Medicine, Toyoake, Japan. [3]Department of Pediatrics, Nagoya University Graduate School of Medicine, Nagoya, Japan. [4]Laboratory for Medical Science Mathematics, RIKEN Center for Integrative Medical Sciences, Yokohama, Japan. [5]Department of Developmental Medicine, Research Institute, Osaka Medical Center for Maternal and Child Health, Izumi, Japan. [6]Department of Pediatrics, Yamagata University Faculty of Medicine, Yamagata, Japan. [7]Department of Medical Genetics, Osaka Medical Center and Research Institute for Maternal and Child Health, Osaka, Japan. [8]Department of Neurosurgery, Takatsuki General Hospital, Osaka, Japan. [9]Division of Regenerative Medicine, Institute for Clinical Research, Osaka National Hospital, National Hospital Organization, Osaka, Japan. [10]Department of Neurosurgery, Osaka National Hospital, National Hospital Organization, Osaka, Japan. [11]Center for Medical Genetics, Keio University School of Medicine, Tokyo, Japan. [12]Department of Pediatrics and Neonatology, Nagoya City University Graduate School of Medical Sciences, Nagoya, Japan. *These authors contributed equally to this work. †Present address: Department of Pediatrics, Showa University School of Medicine, Tokyo, Japan. Correspondence and requests for materials should be addressed to H.K. (email: kura@fujita-hu.ac.jp)

and temporally regulated[11,12]. Mutations in a number of neuronally expressed tubulin genes are associated with a spectrum of cortical development malformations commonly referred to as tubulinopathies. These disorders are caused by mutations in *TUBA1A*[3], *TUBB2B*[4], *TUBB3*[5,6], *TUBB*[7], *TUBB4A*[8], *TUBB2A*[9], and *TUBG1*[10] genes. These mutations thought to involve varying degrees of abnormal neuronal proliferation, migration, and postmigrational development that result in a large spectrum of malformations, including lissencephaly, pachygyria, polymicrogyria, and microcephaly[7,11,13].

Microtubules are ubiquitous structural components that contribute to the cytoskeleton, cilia, flagella, axon fibres, and mitotic spindles[14]. Microtubules are dynamic polymers consisting of tandem repeats of α- and β-tubulin heterodimers, which assemble in a head-to-tail fashion at the growing ends of microtubules. Each microtubule is constructed from 13 laterally connected protofilaments of repeating tubulin heterodimers; lateral interactions between each microtubule form the hollow and cylindrical microtubule body[13,15].

TUBA1A gene encoding α1a-tubulin is expressed in almost all post-mitotic neurons throughout neuronal development. *TUBA1A*-related cortical dysgenesis typically shows a posteriorly predominant lissencephaly with cerebellar hypoplasia (LCH), dysmorphic basal ganglia, thin or absent corpus callosum, congenital microcephaly, ventricular dilatation, and abnormalities of the hippocampus and brainstem[16]. However, the clinical phenotypes caused by *TUBA1A* mutations vary considerably. Recently, *TUBA1A* mutations have also been described in perisylvian asymmetrical polymicrogyria[17–19], polymicrogyria-like cortical dysplasia[20], and microlissencephaly in foetal cases[21]. The clinical manifestations of affected patients often include congenital microcephaly, severe intellectual disability, neurodevelopmental delay with diplegia or tetraplegia, and epilepsy[22].

In our study, we performed whole-exome sequencing of two patients with severe cortical dysgeneses. One patient had an extremely thin cerebral parenchyma apparently looking like hydranencephaly, whereas the other had lissencephaly accompanied by marked hydrocephalus. We identified two novel *de novo* heterozygous *TUBA1A* mutations, c.190 C>T (p.R64W) and c.74 G>T (p.C25F). In addition, we performed a functional assay of the mutant proteins to determine why these patients show more severe phenotypes than patients with classical lissencephaly.

Results

Patients' characteristics. Patient 1 (NCU_F41) was a 3-year-old girl. She was born at a gestational age of 37 weeks by caesarean section. Her parents were healthy and unrelated. Her elder sister was also healthy and had normal development. Her mother was referred to our hospital for foetal growth restriction, microcephaly, and marked ventricular dilatation of her foetus on ultrasonography from 28 weeks of gestation. At patient delivery, the amniotic fluid was excessive but the placenta and umbilical cord were normal. Her Apgar scores were 3 and 5 at 1 and 5 min, respectively. She could not breathe spontaneously and needed mechanical ventilation. Her birth weight was 2116 g (−2.0SD), head circumference was 29.6 cm (−2.4SD), and body length was 44 cm (−1.8SD). She had microcephaly, microphthalmos, widely spaced eyes, and micrognathia. Truncal hypotonia with spastic tetraplegia was evident and her digital joints were contractured.

An ophthalmologic examination revealed bilateral optic nerve hypoplasia. Foetal MRI at 28 weeks of gestation and brain MRI at 6 days after birth revealed an extremely thin cerebral parenchyma, hypoplastic brain stem, and agenesis of the cerebellum and corpus callosum (Fig. 1a–d). Test results for toxoplasma, rubella, cytomegalovirus, and herpes simplex (TORCH) infections were negative. Her karyotype was normal 46, XX. After birth, she presented with focal clonic seizures, sometimes with oxygen desaturation. Her electroencephalogram showed extremely poor background activities and focal rhythmic delta waves during the seizures. As the seizures were treated with phenobarbital, they were partially controlled.

At the age of 1 month, a tracheotomy and tracheal separation were performed because of her recurrent aspiration pneumonia. A gastrostomy and fundoplication were also done at the same time. Because of the agenesis of the pituitary, trichlormethiazide for central diabetes insipidus and hydrocortisone and levothyroxine for hypopituitarism were needed. Since her head circumference had been gradually enlarged, a ventriculoperitoneal shunt was placed at the age of 7 months to control the head growth and to assist in nursing care. At 3 years of age, she had spastic tetraplegia and no definite awareness of her environment.

We performed whole-exome sequencing of peripheral blood DNA from the patient and both her parents (Supplementary Fig. S1a). A *de novo* heterozygous c.190 C>T (p.R64W) variant was identified in *TUBA1A*. Subsequent Sanger sequencing confirmed the presence of this variant in the patient 1 and absence in the genomes of both her parents (Supplementary Fig. S2). The c.190 C>T variant was predicted to be damaging by both PolyPhen-2 and SIFT. No potentially pathogenic variants related to malformations of cortical development were identified in any other genes in patient 1 (Supplementary Table S1).

Patient 2 (K3373) was a 2-year-old boy. Ventricular dilatation was identified in the foetal period. His parents were healthy and unrelated. His elder sister was also healthy and had normal development. He was born at a gestational age of 39 weeks by vaginal delivery. His Apgar scores were 8 and 9 at 1 and 5 min, respectively. His birth weight was 2792 g (−0.9SD), head circumference was 33 cm (−0.2SD), and body length was 49.5 cm (+0.3SD). After birth, he was diagnosed with lissencephaly (Fig. 1e–h). He could breathe and swallow by himself. At the age of 8 months, he began suffering from epileptic spasms,

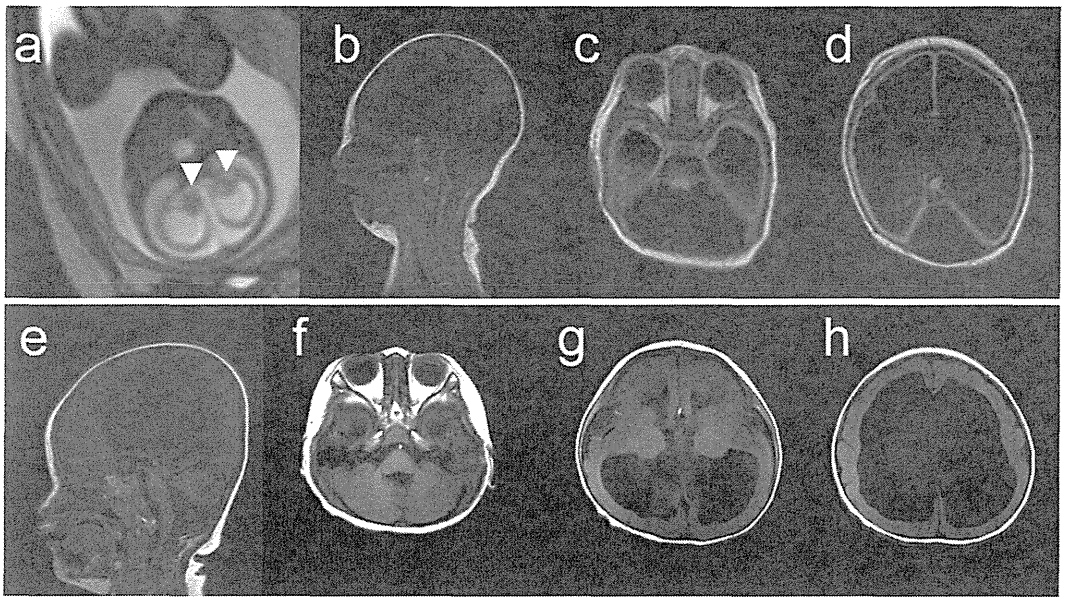

Figure 1. Brain MRI findings of two patients with mutations in *TUBA1A*. (**a**) Foetal MRI at 28 weeks of gestation of patient 1 (T2-weighted image). White arrowheads indicate the basal ganglia. (**b–d**) MRI findings at 6 days after the birth of patient 1 (**b**: T1-weighted image; **c,d**: Fluid Attenuated Inversion recovery [FLAIR]). The patient showed an extremely thin cerebral parenchyma, hypoplastic brain stem, and agenesis of the cerebellum and corpus callosum. Most of the intracranial space was occupied with cerebrospinal fluid. (**e–h**) MRI findings at 1 year of age of patient 2 (T1-weighted images). The patient showed marked ventricular dilatation with a thin cortex, agyria, or limited pachygyria, poorly differentiated dysmorphic basal ganglia, agenesis of the corpus callosum, and slightly hypoplastic cerebellar vermis. The brain stem appeared to be normal.

which could be controlled with sodium valproate and zonisamide. At 2 years of age, he had spastic tetraplegia and was unable to roll over. Although he would not make eye contact and did not speak, he could react to sound and had a smile when his mother called his name.

We performed whole-exome sequencing of peripheral blood DNA from the patient and both his parents (Supplementary Fig. S1b). A *de novo* heterozygous c.74 G>T (p.C25F) variant was identified in *TUBA1A* and confirmed by Sanger methods (Supplementary Fig. S2). This variant was not detected in the genomes of both his parents by Sanger sequencing. The c.74 G>T variant was predicted to be damaging by both PolyPhen-2 and SIFT. There were no potentially pathogenic variants related to malformations of cortical development in any other genes in patient 2 (Supplementary Table S1). Both *TUBA1A* mutations of patients 1 and 2 are located at the amino acids which are conserved across many species (Supplementary Fig. S1c).

Structural modelling of TUBA1A mutations. Both *TUBA1A* mutations reported here are located in the N-terminal domain (Supplementary Fig. S1d) and are predicted to be associated with lateral interactions between microtubules (Fig. 2a–c). According to structural studies conducted using cryoelectron microscopy, protofilaments in microtubules are primarily connected between the M loops and the H1′-S2 and H2-S3 loops[15]. R64 is located on the H1′-S2 loop of α-tubulin (Fig. 2c), which participates in lateral interactions. R64 forms hydrogen bonds with the surrounding residues, E3, F53, and S54 (Fig. 2d). These hydrogen bonds may be involved in the structural stability and/or flexibility of the lateral interactions. Therefore, the R64W mutation is predicted to directly disrupt the lateral interaction. C25 is located on the boundary between helix H1 and the H1-H1′ loop of α-tubulin (Fig. 2c), and this residue faces the luminal side of microtubules (Fig. 2a). The H1-H1′ loop appears to support the H1′-S2 loop and the H2-S3 loop to enhance lateral interactions[15]. Therefore, the C25F mutation may secondarily compromise lateral interactions.

TUBA1A mutants alter the ability of α-tubulin to incorporate into the microtubule network. We examined the ability of the TUBA1A mutants to incorporate into the endogenous microtubule network (Fig. 3). We generated constructs designed to express TUBA1A mutants upon transfection of COS7 cells. The constructs were for wild-type, p.R64W, and p.C25F, as well as p.R402C, which is a recurrent *TUBA1A* mutation that expresses the phenotype of classical lissencephaly, similar to *LIS1* mutations[23]. Transfected cells were examined by immunofluorescence using an anti-FLAG antibody to detect the expression of the transgene and an anti–α-tubulin antibody to detect the overall microtubule network.

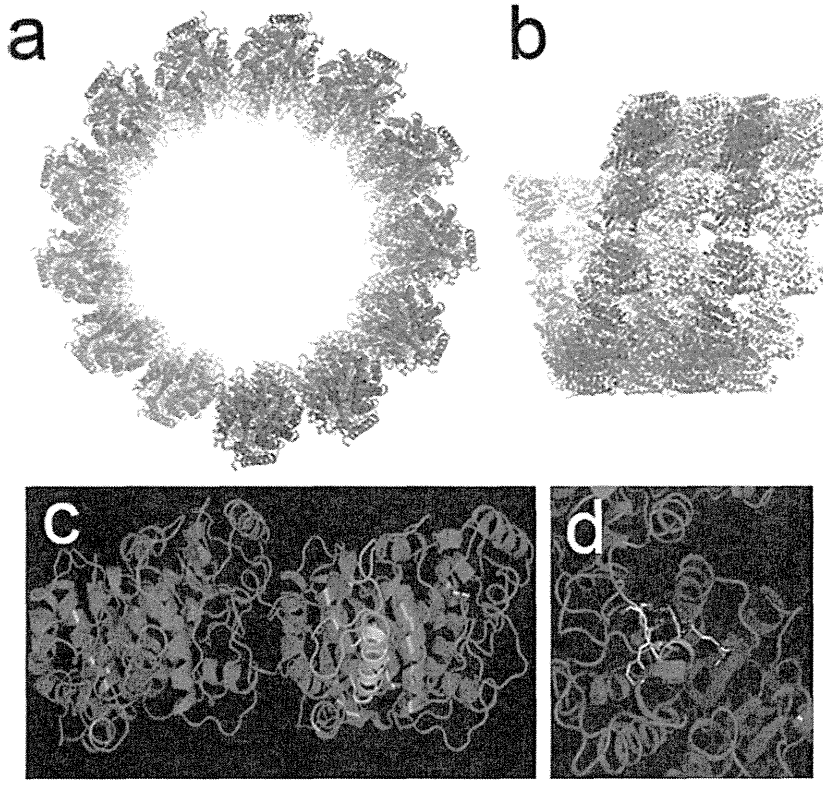

Figure 2. Three-dimensional mapping of *TUBA1A*-mutated residues in a microtubule structure. (**a**) End-on view of a microtubule structural model. A microtubule consists of 13 longitudinal protofilaments that are connected via lateral interactions. α-tubulin molecules are blue, β-tubulin molecules are white, R64 residues are red, and C25 residues are orange. (**b**) Side view of a microtubule. C25 residues are not shown in this view because they are located on the luminal side of a microtubule. (**c**) Higher resolution image of the lateral interaction between the α-tubulin molecules. Both light blue and dark blue are α-tubulin molecules. The M loop is gold, the H1′-S2 loop is red, the H1-H1′ loop is green, and the helix H1 is yellow. The R64 and C25 residues have side chains in this figure. (**d**) The R64 residue forms hydrogen bonds with surrounding residues, E3, F53, and S54.

At 24 h post-transfection, we found that FLAG-tagged wild-type TUBA1A was visualised as lines (Fig. 3a,B) and colocalised with the α-tubulin cytoskeleton (Fig. 3a,C), suggesting that FLAG-tagged wild-type TUBA1A could incorporate into the microtubule network. On the other hand, we found that FLAG-tagged mutant TUBA1A was visible not only as lines, but also as puncta that were diffusely distributed throughout the cytoplasm (Fig. 3a,E,H,K). The linear staining merged with α-tubulin, but the puncta did not colocalise with α-tubulin (Fig. 3a,F,I,L), suggesting that some of the mutant TUBA1A protein could not incorporate into the microtubule network. We observed more incorporated FLAG-tagged TUBA1A protein with R64W and C25F transfection than with R402C. To exclude the influence of the acidic charges of the FLAG tag, we also examined the incorporation of the Myc-tagged TUBA1A protein. Consistent with the data of the FLAG-tagged protein, the incorporation into the microtubule network of Myc-tagged mutant TUBA1A was less than wild-type (Supplementary Fig. S4).

To quantify the incorporation of mutant protein in each transfected cell, we determined the linear staining of FLAG-tagged TUBA1A of each cell by using the ImageJ KBI Line Extract plug-in for line extraction[24] (Supplementary Fig. S3a). These lines indicated the microtubule network of incorporated FLAG-tagged TUBA1A. After line extraction, we measured the total length of the lines and calculated the line density of each cell. The microtubule density of FLAG-tagged TUBA1A for each mutant transfection was analysed.

We found that the microtubule density of FLAG-tagged mutant TUBA1A was significantly lower than that of FLAG-tagged wild-type TUBA1A (Fig. 3b,A). Among TUBA1A mutants, the microtubule density of R64W was the highest, whereas that of R402C was the lowest. We also calculated the microtubule density of α-tubulin in the same manner (Fig. 3b,B). We found that the microtubule density level followed the same order as that of FLAG-tagged TUBA1A. Therefore, the amount of the overall microtubule network tended to depend on the amount of incorporated overexpressed TUBA1A protein. These data indicated that R64W tended to permit higher levels of microtubule incorporation than C25F and R402C. Because there were no significant differences in the mean relative FLAG intensities, the expression levels

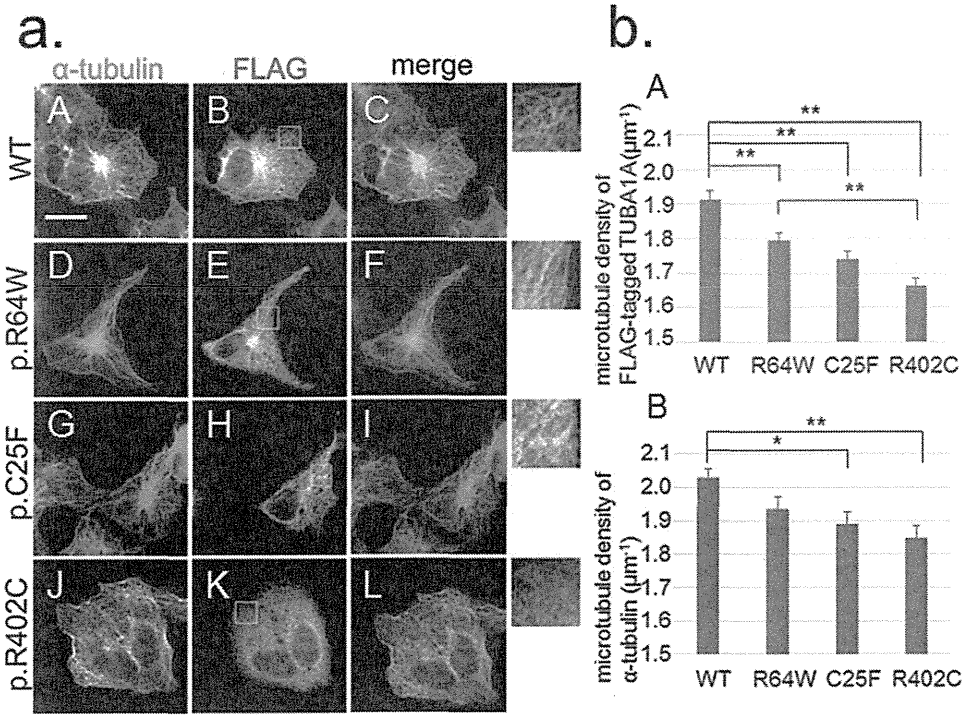

Figure 3. The ability to incorporate into the microtubule network varies among TUBA1A wild-type and mutants. (**a**) Transfected COS7 cells were examined by immunofluorescence using an anti-FLAG antibody (red) and an anti-α-tubulin antibody (green). C-terminal FLAG-tagged wild-type TUBA1A was visualised as lines (B) and colocalised with the cytoskeleton of α-tubulin (C). In the case of FLAG-tagged mutant TUBA1A, there were fewer lines than with the wild-type (E,H,K). Insets are magnified images of the boxes. Scale bar, 20 μm. (**b**) Quantification of microtubule density. We extracted linear staining of FLAG-tagged TUBA1A (A) and the overall cytoskeleton network of α-tubulin (B) of each cell by using the ImageJ KBI Line Extract plug-in and calculated the line density of each cell. Bars represent the means ± SEM (32 cells from wild-type, 28 cells from R64W, 28 cells from C25F, and 31 cells from R402C). Asterisks indicate statistically significant differences (one-way ANOVA and Tukey's post-hoc test; $*p < 0.05$, $**p < 0.01$). (A) The microtubule density of FLAG-tagged mutant TUBA1A was significantly lower than that of FLAG-tagged wild-type TUBA1A. The microtubule density of R64W was the highest among the mutants and that of R402C was the lowest. (B) The microtubule density level of α-tubulin followed the same order as that of FLAG-tagged TUBA1A.

of FLAG-tagged protein in the analysed cells were thought to be similar among wild-type and mutants (Supplementary Fig. S3b).

To assess microtubule dynamics in transfected COS7 cells, we examined repolymerisation after cold induced depolymerisation (Supplementary Fig. S5). There were significantly less cells containing the asters of α-tubulin in the cases of R64W transfection than wild-type (Supplementary Fig. S5c).

TUBA1A mutants alter microtubule stability. We investigated microtubule behaviour in patients' fibroblasts to assess the effects of these mutations on the microtubule stability (Fig. 4). Microtubules of fibroblasts start to depolymerise when they are incubated on ice. We examined the cytoskeleton morphology and the depolymerised tubulin in the fibroblasts by immunofluorescence staining of α-tubulin (Fig. 4a). We first showed by RT-PCR that *TUBA1A* was actually expressed in fibroblasts of the patients and control fibroblasts (control_1) (Supplementary Fig. S6). We defined a cell that contained no linear staining of α-tubulin at 400× magnification to be a completely depolymerised cell. We compared the percentage of completely depolymerised cells between patients' fibroblasts and control ones when they were incubated on ice for 0, 5, 10, 15, and 20 min (Fig. 4b). There were no completely depolymerised control or mutant cells after 0 and 5 min of cold treatment (Fig. 4a,A–F). After 10 min of cold treatment, we found that the percentage of completely depolymerised cells from the R64W and C25F patients was more than four times that of the control (Fig. 4a,G–I,b). The differences for comparison R64W and C25F cells with control cells were statistically significant ($p = 5.6 \times 10^{-24}$ and $p = 5.8 \times 10^{-14}$, respectively, Fig. 4b). This suggested that the depolymerisation of patients' fibroblasts occurred sooner than the control ones. There were almost no differences in the percentage of depolymerised cells after 20 min of cold treatment (Fig. 4a,M–O,b). Repolymerisation of the microtubules could occur in control and mutant

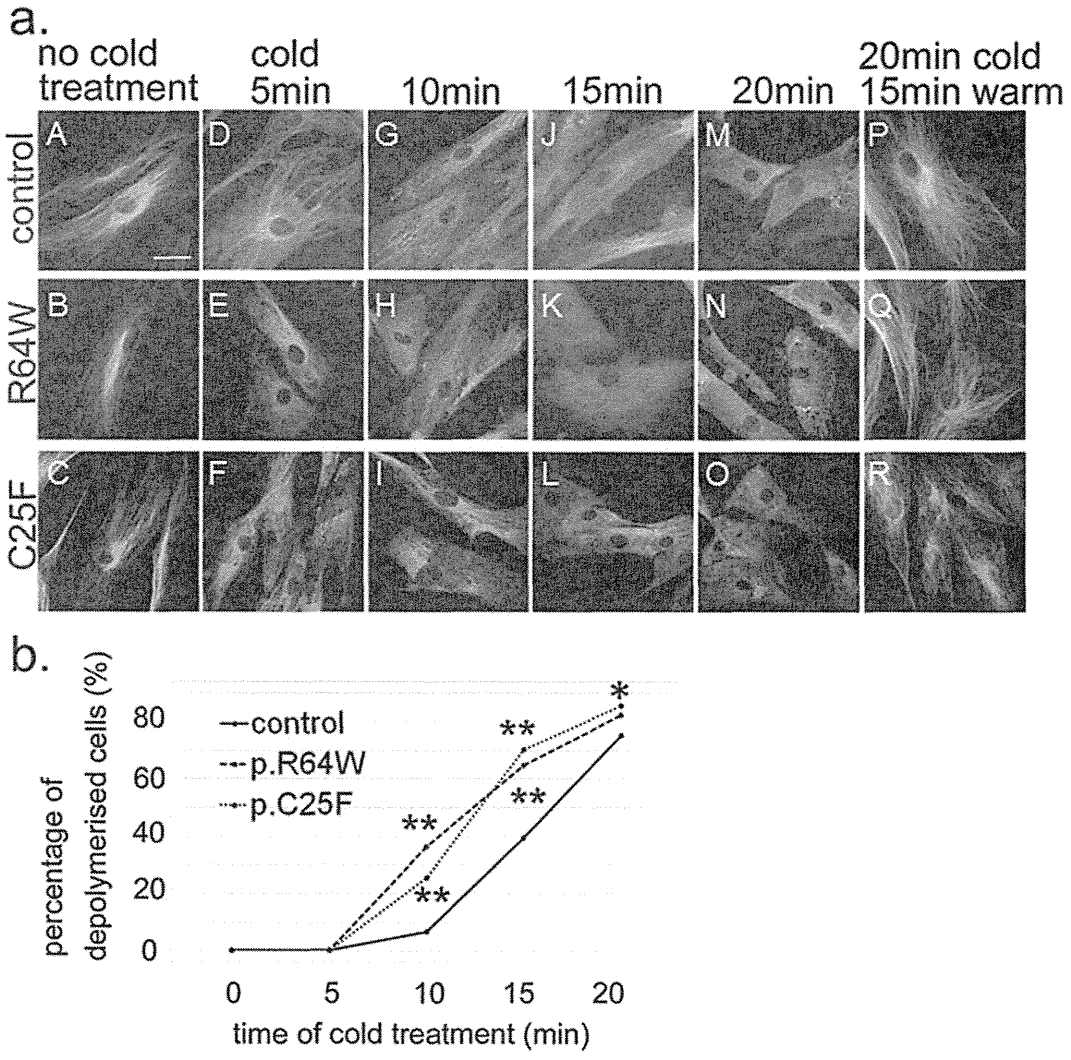

Figure 4. Microtubule behaviour and stability in patients' fibroblasts after various periods of cold treatment. (**a**) Before cold treatment, the cytoskeleton morphologies were similar among control and mutant fibroblasts (A–C). Note that fibroblasts of R64W and C25F were depolymerised after 15 min of cold treatment, whereas polymerised microtubules were still present in control fibroblasts (J–L). Scale bar, 20 μm. (**b**) Percentage of completely depolymerised cells after cold treatment of 0, 5, 10, 15, and 20 min. We counted completely depolymerised cells among 275–400 cells in each condition. After 10 min of cold treatment, the percentage of R64W and C25F fibroblasts showing depolymerisation was more than four times that of control fibroblasts. Asterisks indicate statistically significant differences compared with control (Fisher's exact test and Bonferroni correction using numbers of cells with and without complete depolymerisation, $^{*}p < 0.05$, $^{**}p < 0.0001$).

fibroblasts after treatment on ice for 20 min and subsequently at 37 °C for 15 min (Fig. 4a,P–R) . These data suggested that mutated microtubules are less stable than normal ones.

To assess an underlying mechanism by which *TUBA1A* mutations lead to cortical dysgeneses, we examined the mitosis and the migration of the patients' fibroblasts (Supplementary Fig. S7, S8). There were no significant differences between the patients' and control fibroblasts both in the mitosis and in the migration.

Discussion

In our present study, we identified two novel heterozygous missense *TUBA1A* mutations in patients with severe cortical dysgeneses, one with an extremely thin cerebral parenchyma apparently looking like hydranencephaly and the other with lissencephaly accompanied by marked hydrocephalus. *TUBA1A*-related cortical dysgenesis typically shows a posteriorly predominant lissencephaly with cerebellar hypoplasia (LCH), dysmorphic basal ganglia, thin or absent corpus callosum, congenital microcephaly, ventricular dilatation, and abnormalities of the hippocampus and brainstem[16]. Without these characteristics, it is difficult to determine whether a case with certain brain malformations is a *TUBA1A*-related disorder using

only MRI findings. The brain MRI of our patient harbouring the *TUBA1A* p.R64W mutation manifested an extremely thin cerebral parenchyma with severe hydrocephalus, agenesis of the cerebellum and the corpus callosum, and hypoplastic brain stem, the most severe form of brain malformations. It looked like hydranencephaly but was distinguished from hydranencephaly by the existence of an extremely thin cerebral parenchyma. The cerebral cortex was too thin to assess the layer structure using brain MRI. Thus, our data indicate that the spectrum of *TUBA1A*-related brain malformations is broader than expected.

All previously reported, *TUBA1A* mutations have been heterozygous missense mutations[25,26]. The presence of missense mutations and the absence of nonsense mutations, frameshifts, or whole gene deletions suggest that the mutation results in gain-of-function or has a dominant-negative effect, rather than haploinsufficiency. Among tubulinopathies, it has been proposed that the severity of nervous system impairments may depend on the relative abundance of mutant α- and β-tubulin heterodimers compared with wild-type, combined with their ability to incorporate into the microtubule cytoskeleton, which affect dynamics, motor protein, or MAP interaction in different dominant-negative fashions[13].

In the case of *TUBB3* mutations, R262H substitution permits much more heterodimer formation and microtubule incorporation than R262C, both *in vitro* and in mammalian cells. R262C results in isolated eye movement restrictions, whereas R262H causes not only severe eye movement restrictions, but also other neurological impairments and brain malformations[6]. In the same way, the recurrent R402H mutation in *TUBA1A*, which causes a more severe lissencephaly with complete agyria than R402C, produces a mutant protein that permits higher levels of heterodimer formation and microtubule incorporation than R402C[23,27]. We showed that R64W had the highest amounts of mutant protein incorporation into the network compared with the other mutants and caused the most severe phenotype. In the repolymerisation experiments, the expression of TUBA1A R64W protein impaired the ability of the endogenous α-tubulin to repolymerise. Thus, a greater extent of mutant protein incorporation into the endogenous microtubule network may result in more severe phenotypes in a dominant-negative fashion.

In the current study, the data of the incorporation of FLAG-tagged R402C TUBA1A was different from the previous reports[23,27]. The reason of the difference could be based on the position of the FLAG tag. To exclude the influence of the acidic charges of the FLAG tag, we also examined the incorporation of the Myc-tagged TUBA1A protein. Consistent with the data of the FLAG-tagged protein, limited incorporation of the R402C mutation was observed and the data did not depend on the type of tags. According to the previous report[27], the R402C mutation generated tubulin heterodimers in significantly reduced yield *in vitro* folding reaction. It may be consistent that the R402C mutation disrupts αβ heterodimerisation, leading to little incorporation into the microtubule network.

Tubulin contains three separate structural domains, N-terminal, intermediate, and C-terminal[28] (Supplementary Fig. S1d). These three domains participate in five distinct functions: heterodimer stability, longitudinal and lateral protofilament interactions, nucleotide exchange and hydrolysis, and microtubule–protein interactions[13]. In neurons, lateral interactions are particularly important because microtubules are arranged in dense networks and must be resistant to forces that cause bending or buckling to maintain their structural integrity[13,15,29]. Mutations found at positions essential for lateral interactions are predicted to impede the polymerisation and dynamic properties of microtubules, resulting in microtubules that may be relatively nondynamic or unstable and more likely to depolymerise[13]. In cold-induced depolymerisation of fibroblasts, it is consistent that the two TUBA1A mutants, R64W and C25F, could make microtubules less stable than those of the controls by disrupting lateral interactions.

We investigated the severity of *TUBA1A*-related cortical dysgeneses that are associated with lateral interactions in previous reports as well as in this report. *TUBA1A* mutations that primarily participate in lateral interactions include L286F[30] (M loop), E55K[31], T56M[25], R64W (H1′-S2 loop), and L92V[23] (H2-S3 loop). The patients harbouring L286F, T56M, and L92V were foetuses. Using the classification of Kumar *et al.*[23], four mutations (L286F, T56M, R64W, and L92V) are classified in the severe lissencephaly with cerebellar hypoplasia (LCH severe group 4). On the other hand, E55K belongs to the moderate lissencephaly (LIS moderate group 1) with extreme microcephaly. There are also neighbouring loops that may support lateral interactions. The H1-H1′ loop supports the H1′-S2 loop and the H2-S3 loop, and the end of H6 and the S9-S10 loop appear to stabilise the M loops[15]. *TUBA1A* mutations that secondarily participate in lateral interactions include C25F, E27Q[26] (H1-H1′ loop), Y210C[17], D218Y[23] (the end of H6), G366R[32], A369T[25], and V371E[25] (S9–S10 loop). Five mutations (E27Q, Y210C, D218Y, G366R, and V371E) were classified into the LCH severe group 4 and C25F resembled the LCH severe group 4 phenotype except for milder cerebellar vermis hypoplasia. Only A369T showed central pachygyria. Therefore, many of the reported *TUBA1A* mutations at positions associated with lateral interactions caused severe phenotypes of brain malformations (LCH severe group 4).

In the case of β-tubulin, R62 of TUBB3 is also positioned in the H1′-S2 loop of β-tubulin and is predicted to participate in lateral interactions[6]. However, patients harbouring R62Q have a milder phenotype among TUBB3 mutations. As it was reported that residues involved in lateral interactions cluster in regions of divergence between species and marked difference between α- and β-tubulins[28], there may be different consequences for α- and β-tubulins when lateral interactions are disrupted. We propose that the differences in clinical manifestations among tubulinopathies caused by a mutated tubulin gene should be evaluated.

In conclusion, our data suggest that mutations in *TUBA1A* at positions essential for lateral interactions may lead to severe phenotypes of brain malformations. However, we did not show the consequences

of these mutants for neuronal developmental processes such as proliferation, migration, differentiation, and axonal guidance. In patients' fibroblasts, the mitosis and the migration were not impaired. Further studies of how each mutant affects microtubule function and how it impairs neuronal developmental processes will reveal the precise function of microtubules in normal neuronal development.

Methods

Patients. Genetic testing was approved by the ethical committees of Fujita Health University and collaborated institutes in accordance with the principles of the Declaration of Helsinki, and the Ethical Guidelines for Human Genome/Gene Analysis Research by the Ministry of Education, Culture, Science, and Technology, the Ministry of Health, Labor, and Welfare, and the Ministry of Economy, Trade, and Industry of Japan. Blood samples from affected individuals and their parents, and skin biopsy samples were obtained with informed consent according to local institutional review board guidelines.

Whole-exome sequencing and validation. Genomic DNA was extracted from peripheral blood using the QIAamp DNA Blood Midi Kit according to the manufacturer's instructions (Qiagen, Tokyo, Japan). Three micrograms of DNA were sheared into 150–200-bp fragments using theM220 Focused-ultrasonicator (Covaris, Woburn, MAUSA). To capture the exonic DNA, we used the SureSelect XT Human All Exon V5 capture library (Agilent Technologies, Santa Clara, CAUSA). We then constructed a sequence library using the SureSelect XT Target Enrichment System for the Illumina Paired-End Sequencing Library kit (Agilent Technologies) and performed DNA sequencing of 100-bp paired-end reads using the Illumina HiSeq 2000 sequencer. The sequencing data were mapped to the reference genome (GRCh37/hg19) using BWA (ver.0.6.1). Variant calling was performed using SAMtools (ver.0.1.16) and GATK (ver.1.6) software as previously reported[33]. To identify disease causative mutations, we excluded known variants found in public databases (dbSNP138, 1000 Genomes Project, NHLBI ESP6500, and Exome Aggregation Consortium [ExAC]) and a control in-house database, except for those also identified as pathogenic mutations in the NCBI ClinVar and HGMD databases. We focused on non-synonymous single nucleotide variants (SNVs), insertions and deletions (indels), and splice site variants. Predictions of possible impact of amino acid substitution on the structure and function by variant were performed using PolyPhen-2[34] and SIFT[35] software. The mutations were confirmed by Sanger sequencing.

Structural modelling of TUBA1A mutations. Tubulin dimer structure (PDB ID:1JFF) docked into the density map (MT-13-3, EMDB ID: EMD-5193) using Chimera (https://www.cgl.ucsf.edu/chimera/) after the homology modelling of missing residues 35–60 in α-tubulin was kindly provided by Dr. Haixin Sui, New York State Department of Health[15]. Polymerised microtubule images were then generated with Chimera and MolFeat (FiatLux, Tokyo, Japan).

Transfection experiments. The full-length cDNA encoding the human *TUBA1A* sequence was generated by PCR using a template from placenta cDNA (Forward primer: 5′-TAAGCGGCCGCCATG CGTGAGTGCATCTCCATCCAC-3′, Reverse primer: 5′-TAACTGCAGGTATTCCTCTCCTTCTTCC TCACCCTC-3′). The PCR product was cloned into the *Not* I and *Pst* I sites of the pCMV-4A vector (Agilent Technologies), which is a mammalian expression vector for tagging proteins with a C-terminal FLAG (DYKDDDDK) epitope under the control of the CMV promoter. Three mutations—p.R64W, p.C25F, and p.R402C—were generated by PCR using a template of the wild-type construct. For construction of the Myc tag vectors, the *Xho* I and *Apa* I fragment of these FLAG tag constructs were replaced with a synthesized DNA encoding a Myc tag (The fragment sequence is 5′-TCGAGGAACAAAAACTCATCTCAGAAGAGGATCTGTAGGGCC-3′). All constructs were checked by DNA sequencing.

Constructs were transfected into COS7 cells grown on glass coverslips in Opti-MEM I using Lipofectamine 2000 (Life Technologies). At 24 h after transfection, cells were fixed with ice-cold methanol and stained with a mouse monoclonal anti–α-tubulin antibody (Santa Cruz Biotechnology) and a goat polyclonal anti-DYKDDDDK antibody (Novus Biologicals) at dilutions of 1:250 and 1:5000, respectively. Secondary antibodies were donkey anti-mouse IgG Alexa Fluor 488 and donkey anti-goat IgG Alexa Fluor 594 (Life Technologies) at dilutions of 1:1000. In repolymerisation experiments of COS7 cells[35], cells were incubated on ice for 30 min and then restored to 37 °C for 1.5 min. Cells were immediately fixed with ice-cold methanol and stained as above. For the Myc tag experiment, a rabbit polyclonal anti-Myc antibody (MBL) at dilution of 1:100 and donkey anti-rabbit IgG Alexa Fluor 594 (Life Technologies) at dilutions of 1:1000 were used.

RT-PCR. RT-PCR was done by manufacturer's protocol. NucleoSpin RNA II (MACHEREY-NAGEL) and SuperScript III First-Strand Synthesis System (Life Technologies) were used. The primer sequences of *TUBA1A* and *HPRT* are shown in the Supplementary Figure S6.

Depolymerisation experiments of fibroblasts. Fibroblasts were derived from skin biopsies taken from the patients with p.R64W and p.C25F mutations and control people. The depolymerisation experiments were done as previously described[5]. Briefly, fibroblasts (passage 3) grown on glass coverslips in

IMDM containing 10% foetal bovine serum, penicillin 50 U/ml and streptomycin 50 ug/ml were incubated for 0, 5, 10, 15, and 20 min on ice and fixed. Repolymerisation experiments of fibroblasts were performed by incubating cells on ice for 20 min and then restoring them to 37 °C for 15 min. Cells were stained with a mouse monoclonal anti-α-tubulin antibody used at a dilution of 1:100. The secondary antibody was donkey anti-mouse IgG Alexa Fluor 488 used at a dilution of 1:1000.

Mitotic Index and mitotic spindle formation. Fibroblasts (passage 5) grown on glass coverslips were fixed with ice-cold methanol and stained with a mouse monoclonal anti-α-tubulin antibody and a rabbit polyclonal anti-phospho Histone H3 (pH3) (Ser10) antibody (MILLIPORE) at dilutions of 1:250 and 1:100, respectively. Secondary antibodies were donkey anti-mouse IgG Alexa Fluor 488 and donkey anti-rabbit IgG Alexa Fluor 594 (Life Technologies) at dilutions of 1:1000. The pH3 signal-positive mitotic fibroblasts were counted from at least 830 total cells.

***In vitro* scratch assay.** The *in vitro* scratch assay was done as previously described[37]. For each image, distances between one side of scratch and the other were measured using ImageJ and 50 readings of distances were measured for each sample.

Image acquisition. Slides were observed under a fluorescence microscope (Axio Imager M1; Carl Zeiss) equipped with a digital camera (AxioCam HRc; Carl Zeiss). COS7 cells and fibroblasts were observed at 630× and 400× magnifications, respectively. *In vitro* scratch assay, dishes were observed under Axiovert 200M (Carl Zeiss) equipped with a digital camera (AxioCam MRm; Carl Zeiss) and fibroblasts were observed at a 100× magnification. Images were captured with the same settings using AxioVision 4.8 software (Carl Zeiss).

Quantification of microtubule density and relative FLAG intensity. Quantification of microtubule density was performed as previously described[24]. For each COS7 cell, a region of interest (ROI) was manually assigned along the edge of the cell by the free hand tool in ImageJ. We then calculated the area and the mean intensity of the ROI by using the ImageJ ROI manager. We used the KBI Line Extract plug-in for line extraction. The parameters were giwsIter 5, mdnmsLen 20, pickup above 0.0, shaven Len 5, and del Len 5. The total length of the extracted lines was calculated by the KBI Line Feature plug-in in ImageJ for the α-tubulin staining and the FLAG staining. The total length of the extracted lines in a selected cell divided by the area of the cell gave the microtubule density. These plug-ins are available as part of the KBI ImageJ plug-in package (http://hasezawa.ib.k.u-tokyo.ac.jp/zp/Kbi/ImageJKbiPlugins). The relative FLAG intensity was determined in ImageJ by subtracting the mean red signal intensity of an untransfected cell from that of a transfected cell. The untransfected cell was in the same image as that of the transfected cell.

Statistical analysis. One-way ANOVA and Tukey's post-hoc analysis and a chi-square test were performed using IBM SPSS Statistics Version 22. Fisher's exact test and the Bonferroni correction were performed using R software. We considered $p < 0.05$ to be significant after correction.

References

1. Barkovich, A. J., Guerrini, R., Kuzniecky, R. I., Jackson, G. D. & Dobyns, W. B. A developmental and genetic classification for malformations of cortical development: update 2012. *Brain* **135,** 1348–1369 (2012).
2. Kerjan, G. & Gleeson, J. G. Genetic mechanisms underlying abnormal neuronal migration in classical lissencephaly. *Trends Genet* **23,** 623–630 (2007).
3. Keays, D. A. *et al.* Mutations in alpha-tubulin cause abnormal neuronal migration in mice and lissencephaly in humans. *Cell* **128,** 45–57 (2007).
4. Jaglin, X. H. *et al.* Mutations in the beta-tubulin gene TUBB2B result in asymmetrical polymicrogyria. *Nat Genet* **41,** 746–752 (2009).
5. Poirier, K. *et al.* Mutations in the neuronal ss-tubulin subunit TUBB3 result in malformation of cortical development and neuronal migration defects. *Hum Mol Genet* **19,** 4462–4473 (2010).
6. Tischfield, M. A. *et al.* Human TUBB3 mutations perturb microtubule dynamics, kinesin interactions, and axon guidance. *Cell* **140,** 74–87 (2010).
7. Breuss, M. *et al.* Mutations in the beta-tubulin gene TUBB5 cause microcephaly with structural brain abnormalities. *Cell Rep* **2,** 1554–1562 (2012).
8. Simons, C. *et al.* A *de novo* mutation in the beta-tubulin gene TUBB4A results in the leukoencephalopathy hypomyelination with atrophy of the basal ganglia and cerebellum. *Am J Hum Genet* **92,** 767–773 (2013).
9. Cushion, T. D. *et al. De novo* mutations in the beta-tubulin gene TUBB2A cause simplified gyral patterning and infantile-onset epilepsy. *Am J Hum Genet* **94,** 634–641 (2014).
10. Poirier, K. *et al.* Mutations in TUBG1, DYNC1H1, KIF5C and KIF2A cause malformations of cortical development and microcephaly. *Nat Genet* **45,** 639–647 (2013).
11. Jaglin, X. H. & Chelly, J. Tubulin-related cortical dysgeneses: microtubule dysfunction underlying neuronal migration defects. *Trends Genet* **25,** 555–566 (2009).
12. Miller, F. D. *et al.* Isotypes of alpha-tubulin are differentially regulated during neuronal maturation. *J Cell Biol.* **105,** 3065–3073 (1987).
13. Tischfield, M. A., Cederquist, G. Y., Gupta, M. L., Jr. & Engle, E. C. Phenotypic spectrum of the tubulin-related disorders and functional implications of disease-causing mutations. *Curr Opin Genet Dev* **21,** 286–294 (2011).
14. Jackson, A. P. Diversifying microtubules in brain development. *Nat Genet* **41,** 638–640 (2009).

15. Sui, H. & Downing, K. H. Structural basis of interprotofilament interaction and lateral deformation of microtubules. *Structure* **18,** 1022–1031 (2010).
16. Fry, A. E., Cushion, T. D. & Pilz, D. T. The genetics of lissencephaly. *Am J Med Genet C Semin Med Genet* **166C,** 198–210 (2014).
17. Jansen, A. C. *et al.* TUBA1A mutations: from isolated lissencephaly to familial polymicrogyria. *Neurology* **76,** 988–992 (2011).
18. Poirier, K. *et al.* Expanding the spectrum of TUBA1A-related cortical dysgenesis to Polymicrogyria. *Eur J Hum Genet* **21,** 381–385 (2013).
19. Zanni, G. *et al.* Description of a novel TUBA1A mutation in Arg-390 associated with asymmetrical polymicrogyria and mid-hindbrain dysgenesis. *Eur J Paediatr Neurol* **17,** 361–365 (2013).
20. Cushion, T. D. *et al.* Overlapping cortical malformations and mutations in TUBB2B and TUBA1A. *Brain* **136,** 536–548 (2013).
21. Fallet-Bianco, C. *et al.* Mutations in tubulin genes are frequent causes of various foetal malformations of cortical development including microlissencephaly. *Acta Neuropathol Commun* **2,** 69 (2014).
22. Bahi-Buisson, N. *et al.* Refinement of cortical dysgeneses spectrum associated with TUBA1A mutations. *J Med Genet* **45,** 647–653 (2008).
23. Kumar, R. A. *et al.* TUBA1A mutations cause wide spectrum lissencephaly (smooth brain) and suggest that multiple neuronal migration pathways converge on alpha tubulins. *Hum Mol Genet* **19,** 2817–2827 (2010).
24. Fujita, S. *et al.* An atypical tubulin kinase mediates stress-induced microtubule depolymerization in Arabidopsis. *Curr Biol* **23,** 1969–1978 (2013).
25. Bahi-Buisson, N. *et al.* The wide spectrum of tubulinopathies: what are the key features for the diagnosis? *Brain* **137,** 1676–1700 (2014).
26. Shimojima, K. *et al.* Whole-exome sequencing identifies a *de novo* TUBA1A mutation in a patient with sporadic malformations of cortical development: a case report. *BMC Res Notes* **7,** 465 (2014).
27. Tian, G. *et al.* Disease-associated mutations in TUBA1A result in a spectrum of defects in the tubulin folding and heterodimer assembly pathway. *Hum Mol Genet* **19,** 3599–3613 (2010).
28. Lowe, J., Li, H., Downing, K. H. & Nogales, E. Refined structure of alpha beta-tubulin at 3.5 A resolution. *J Mol Biol* **313,** 1045–1057 (2001).
29. Brangwynne, C. P. *et al.* Microtubules can bear enhanced compressive loads in living cells because of lateral reinforcement. *J Cell Biol* **173,** 733–741(2006).
30. Poirier, K. *et al.* Large spectrum of lissencephaly and pachygyria phenotypes resulting from *de novo* missense mutations in tubulin alpha 1A (TUBA1A). *Hum Mutat* **28,** 1055–1064 (2007).
31. Morris-Rosendahl, D. J. *et al.* Refining the phenotype of alpha-1a Tubulin (TUBA1A) mutation in patients with classical lissencephaly. *Clin Genet* **74,** 425–433 (2008).
32. Okumura, A. *et al.* Lissencephaly with marked ventricular dilation, agenesis of corpus callosum, and cerebellar hypoplasia caused by TUBA1A mutation. *Brain Dev* **35,** 274–279 (2013).
33. Okamoto, N. *et al.* KIF1A mutation in a patient with progressive neurodegeneration. *J. Hum. Genet.* **59,** 639–641 (2014).
34. Adzhubei, I. A. *et al.* A method and server for predicting damaging missense mutations. *Nat. Methods* **7,** 248–249 (2010).
35. Kumar, P. *et al.* Predicting the effects of coding non-synonymous variants on protein function using the SIFT algorithm. *Nat. Protoc.* **4,** 1073–1081 (2009).
36. Bradley, N. S. *et al.* Exome-wide rare variant analysis identifies TUBA4A mutations associated with familial ALS. *Neuron.* **84,** 324–331 (2014).
37. Chun-achi, L. *et al. In vitro* scratch assay: a convenient and inexpensive method for analysis of cell migration *in vitro*. *Nat. Protoc.* **2,** 329–333 (2007).

Acknowledgments

This study was supported in part by a grant for Research on Applying Health Technology from the Ministry of Health, Labour and Welfare of Japan to F.M., N.O., M.K., M.Y., Y.K., K.K. and S.S.; by SENTAN, JST, Japan to I.Y. We thank the families and M. Hayakawa for their involvement and participation; H. Sui for the kind gift of the structural modelling data; and H. Inagaki, T. Ohye, T. Kato, and S. Yokoi for helpful discussions. We thank Mr. K. A. Boroevich for English proofreading.

Author Contributions

S.Y., M.T. and N.F. performed all experiments except whole-exome sequencing. F.M. performed whole-exome sequencing and the analysis. M.K., N.O., T.T., M.Y., Y.K., K.K. and S.S. participated in whole-exome sequencing. N.I., H.Y., S.K. and J.N. contributed materials. I.Y. constructed the microtubule structural model (Fig. 2). S.Y., N.I. and H.K. wrote the manuscript. All authors reviewed the manuscript.

Additional Information

Supplementary information accompanies this paper at http://www.nature.com/srep

Competing financial interests: The authors declare no competing financial interests.

How to cite this article: Yokoi, S. *et al. TUBA1A* mutation can cause a hydranencephaly-like severe form of cortical dysgenesis. *Sci. Rep.* **5**, 15165; doi: 10.1038/srep15165 (2015).

OPEN

Citation: Human Genome Variation (2015) **2**, 15007; doi:10.1038/hgv.2015.7

www.nature.com/hgv

DATA REPORT

Truncating mutation in *NFIA* causes brain malformation and urinary tract defects

Yutaka Negishi[1,10], Fuyuki Miya[2,10], Ayako Hattori[1], Kentaro Mizuno[3], Ikumi Hori[1], Naoki Ando[1], Nobuhiko Okamoto[4], Mitsuhiro Kato[5], Tatsuhiko Tsunoda[2], Mami Yamasaki[6], Yonehiro Kanemura[7,8], Kenjiro Kosaki[9] and Shinji Saitoh[1]

Chromosome 1p32-p31 deletion syndrome involving the *Nuclear factor I/A* (*NFIA*) gene is characterized by corpus callosum hypoplasia or defects and urinary tract defects. Herein we report on a case resembling the 1p32-p31 deletion syndrome carrying a *de novo* truncating mutation (c.1094delC; p.Pro365Hisfs*32) in the *NFIA* gene, confirming that haploinsufficiency of the *NFIA* gene is a major determinant of this syndrome.

Human Genome Variation (2015) **2,** 15007; doi:10.1038/hgv.2015.7; published online 26 February 2015

Chromosome 1p32-p31 deletion syndrome (OMIM #613735) involving the *Nuclear factor I/A* (*NFIA*) gene is characterized by corpus callosum hypoplasia or defects, hydrocephalus or ventricular enlargement and urinary tract defects.[1] Only six cases of this contiguous gene-deletion syndrome have been reported in the literature.[1–5] Additionally, Lu *et al.*[1] reported two patients showing a similar phenotype, but with balanced translocations breakpoints in the *NFIA* gene.[6] These authors also demonstrated ventricular enlargement, callosal agenesis and urinary tract defects in homozygous $Nfia^{-/-}$ mice and heterozygous $Nfia^{+/-}$ mice.[1] Recently, Rao *et al.*[7] reported a case exhibiting a similar phenotype with an intragenic deletion in the *NFIA* gene, but no structural chromosomal abnormalities detected by CGH microarray. Although haploinsufficiency of the *NFIA* gene is considered the main contributor to the phenotype of this chromosome 1p32-p31 deletion syndrome, the evidence is not conclusive because no single nucleotide variant (SNV) in the *NFIA* gene has been identified and chromosomal rearrangements including deletion or translocation could have a position effect disturbing the proper expression of the neighboring genes.

We herein report on a case of an individual showing interhemispheric cysts, ventricular enlargement, callosal agenesis and urinary tract defects, and carrying a heterozygous *de novo* frameshift mutation in the *NFIA* gene. These findings provide further strong evidence that haploinsufficiency of the *NFIA* gene is a main contributor of 1p32-p31 deletion syndrome, and the *NFIA* gene has a fundamental role in development of brain as well as urinary tract.

This study was approved by the institutional review board of Nagoya City University Graduate School of Medical Sciences.

The proband is a 5-year-old boy with no family history of the relevant diseases. Callosal agenesis was suspected from the 28th gestational week of the fetal period. The boy was born by cesarean section on the 41st gestational week due to enlargement of the head circumference and post-term pregnancy. His Apgar score was 9 at 5 min post partum, his weight was 3180 g (+0.4 s.d.) and his head circumference was 38.2 cm (+3.3 s.d.). No apparent external malformations were observed. Head magnetic resonance imaging (MRI) on the third day of life revealed interhemispheric cysts, ventricular enlargement and callosal agenesis; however, he was in good general condition. Regarding his developmental milestones, he was able to hold his head up by 4 months and started walking without support at 1 year and 3 months. He was observed speaking meaningful words at 2 years and 1 month, showing a slight delay in language, and his intelligence quotient at 4 years measured by the Tanaka–Binet Intelligence Scale was 75. No epileptic seizures have been observed to date, although electroencephalogram detected sharp waves in the frontal head area at 11 months. A follow-up MRI at 4 years revealed polymicrogyria in the right frontal lobe, while the size of the interhemispheric cysts, longitudinal cerebral fissure and ventricular system remained unchanged (Figures 1a,b). Although no abnormal signals were observed in the spinal cord in a spine MRI carried out at 5 years, cystectasia and left hydronephrosis were observed. A voiding cysturethrogram performed at 5 years showed bilateral grade IV vesicoureteral reflux (Figure 1c). His current head circumference is 56.1 cm (+3.8 s.d.) showing non-progressive enlargement of head circumference. He showed only a little dysmorphic facial features including mild macrocephaly, high forehead, and thin upper lip (Figure 1d).

We performed a whole-exome sequencing on the proband and his parents (Figure 2a). To do this, genomic DNA was extracted from peripheral blood using the QIAamp DNA Blood Midi Kit according to the manufacturer's instructions (Qiagen, Tokyo, Japan). Three micrograms of DNA was sheared into 150-200-bp fragments using the Covaris DNA Shearing service (Covaris,

[1]Department of Pediatrics and Neonatology, Nagoya City University Graduate School of Medical Sciences, Nagoya, Japan; [2]Laboratory for Medical Science Mathematics, RIKEN Center for Integrative Medical Sciences, Yokohama, Japan; [3]Department of Nephro-Urology, Nagoya City University Graduate School of Medical Sciences, Nagoya, Japan; [4]Department of Medical Genetics, Osaka Medical Center and Research Institute for Maternal and Child Health, Osaka, Japan; [5]Department of Pediatrics, Yamagata University Faculty of Medicine, Yamagata, Japan; [6]Department of Neurosurgery, Takatsuki General Hospital, Osaka, Japan; [7]Division of Regenerative Medicine, Institute for Clinical Research, Osaka National Hospital, National Hospital Organization, Osaka, Japan; [8]Department of Neurosurgery, Osaka National Hospital, National Hospital Organization, Osaka, Japan and [9]Center for Medical Genetics, Keio University School of Medicine, Tokyo, Japan.
Correspondence: S Saitoh (ss11@med.nagoya-cu.ac.jp)
[10]These authors contributed equally to this work.
Received 1 September 2014; revised 26 November 2014; accepted 25 December 2014

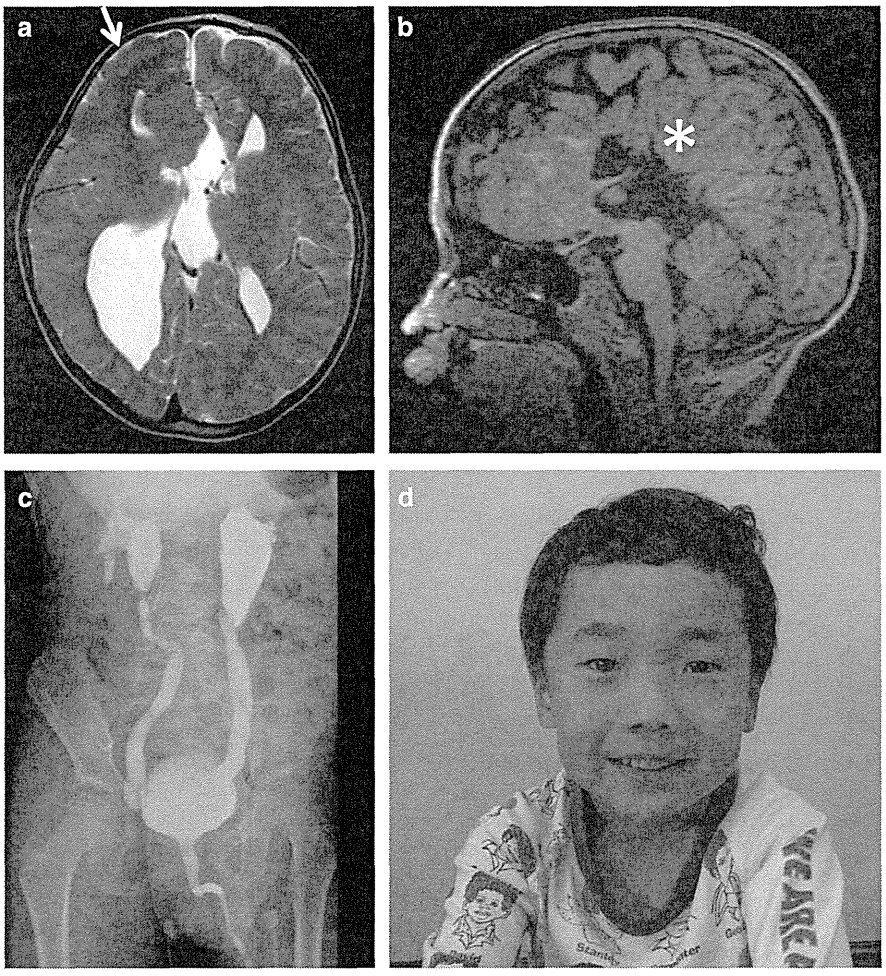

Figure 1. Head MRI, voiding cysturethrogram (VCUG) and craniofacial appearance of our patient. (**a**) Axial T2-weighted image showing interhemispheric cysts, ventricular enlargement and polymicrogyria (arrow). (**b**) Mid-sagittal T1-weighted image showing callosal agenesis (asterisk). (**c**) The VCUG showed bilateral grade IV vesicoureteral reflux. (**d**) Representative photograph of the patient showing a little dysmorphic facial features including mild macrocephaly, high forehead, and thin upper lip. His parents gave informed consent for publication of this image.

Woburn, MA, USA). To capture the exonic DNA, we used the SureSelect XT Human All Exon V5 capture library (Agilent Technologies, Santa Clara, CA, USA). We then constructed a sequence library using the SureSelect XT Target Enrichment System for Illumina Paired-End Sequencing Library kit (Agilent Technologies), and performed DNA sequencing of 100-bp paired-end reads by using the Illumina HiSeq 2000 sequencer (Illumina, San Diego, CA, USA). On average, we obtained 5.85 Gb of sequence reads. The sequencing data was mapped to a reference genome (GRCh37/hg19) using Burrows-Wheeler Alignment tool (ver.0.6.1; http://www.bio-bwa.sourceforge.net/), and the average read depth of targeted regions was 67.5. Variant calling was performed using SAMtools (ver.0.1.16; http://www.samtools.sourceforge.net/) and GATK (ver.1.6; http://www.broadinstitute.org/gatk/) software. To identify the disease causative mutations, we excluded known variants found in public databases (dbSNP138, 1000 Genomes Project, and NHLBI ESP6500) and a control in-house database (154 Japanese individuals of normal and other diseases control), except for those also identified as pathogenic mutations in the NCBI ClinVar (http://www.ncbi.nlm.nih.gov/clinvar/) and HGMD databases (http://www.hgmd.org/). We focused on non-synonymous SNVs, insertions and deletions (indels), and splice-site variants (Figure 2b). This analysis revealed a heterozygous frameshift mutation (c.1094delC; p.Pro365-Hisfs*32) in the *NFIA* gene (NM_001134673.3), which is absent in his parents, indicating that the mutation arose *de novo* (Figure 2c). The mutation was confirmed by Sanger sequencing (Figure 2d). This deletion led to an open reading frameshift that introduced an early stop codon which truncated 114 aminoacids. Consequently, a truncated NFIA protein is generated by this mutation.

The *NFIA* gene has four transcriptional variants in human. Functional significance of each isoform has not been clarified. Only isoform 2 lacks an alternative exon downstream of the identified deletion site (Supplementary Figure a). The c.1094delC mutation would create protein truncation in each isoform. To examine the expression level of each transcript PCR with reverse transcription reaction was performed by using RNA isolated from normal human brain tissues (adult cortex, cerebellum, spinal cord and fetal brain). *NFIA* isoform 2 transcript was less predominant compared with isoforms 1, 3 and 4 (Supplementary Figure b). Therefore, the c.1094delC mutation would induce more effects on longer isoforms 1, 3 and 4 than on isoform 2, and the exon of deletion site and/or next exon which are used in all wild-type isoforms as translation regions would have an important role in NFIA protein.

Three molecular mechanisms are known to cause the complex central nervous system malformation syndrome associated with the *NFIA* gene: (1) interstitial deletion of chromosome 1p32-p31 involving the *NFIA* gene; (2) translocations of chromosome 1p32-p31 involving the *NFIA* gene; and (3) intragenic deletion in